Carbon sequestration in an expanding lake system during the Toarcian Oceanic Anoxic Event

Weimu Xu[1]*, Micha Ruhl[1], Hugh C. Jenkyns[1], Stephen P. Hesselbo[2], James B. Riding[3], David Selby[4], B. David A. Naafs[5], Johan W.H. Weijers[6], Richard D. Pancost[5], Erik W. Tegelaar[6], Erdem F. Idiz[1]

[1]Department of Earth Sciences, University of Oxford, Oxford OX1 3AN, UK (*Correspondence: weimu.xu@earth.ox.ac.uk)

[2]Camborne School of Mines, University of Exeter, Penryn TR10 9FE, UK

[3]British Geological Survey, Keyworth, Nottingham NG12 5GG, UK

[4]Department of Earth Sciences, University of Durham, Durham DH1 3LE, UK

[5]Organic Geochemistry Unit, School of Chemistry and Cabot Institute, University of Bristol, Bristol BS8 1TS, UK

[6]Shell Global Solutions International B.V., Rijswijk 2288 GS, The Netherlands

The Early Jurassic Toarcian Oceanic Anoxic Event (~183 Ma) was marked by marine anoxia–euxinia and globally significant organic-matter burial, accompanied by a major global carbon-cycle perturbation probably linked to Karoo-Ferrar volcanism. Although the Toarcian Oceanic Anoxic Event is well studied in the marine realm, accompanying climatic and environmental change on the continents is poorly understood. Here, utilizing radiometric, palynological and geochemical data from lacustrine black shales, we demonstrate that a major lake system developed contemporaneously with the Toarcian Oceanic Anoxic Event in the Sichuan Basin, China, likely due to enhanced hydrological cycling under elevated atmospheric pCO_2. Coeval accelerated organic-carbon burial in both marine and lacustrine basins suggests nutrient delivery as the prime cause for global carbon-cycle recovery during the Toarcian Oceanic Anoxic Event. Increased lacustrine organic productivity from elevated fluvial nutrient supply resulted in the burial of ~460 Gt of organic carbon in the Sichuan Basin alone, creating an important negative feedback in the global exogenic carbon cycle, which significantly shortened the global $\delta^{13}C$ recovery.

The early Toarcian Oceanic Anoxic Event (T-OAE at ~183 Ma) is recognized as one of the most intense and geographically extensive events of oceanic redox change and accompanying organic-carbon burial in the Mesozoic Era[1,2]. The T-OAE is marked by major changes in global geochemical cycles, with an apparently rapid negative shift of as much as ~7‰ in bulk marine and terrestrial organic-carbon isotope records and a typically smaller (3–6‰) negative excursion in carbonate archives and specific organic compounds[3-10]. The observed early Toarcian perturbation to the exogenic carbon cycle has been linked to volcanism of the Karoo-Ferrar large igneous province (LIP) and associated release of volcanogenic CO_2, thermogenic methane (CH_4) from sill intrusion into Gondwanan coals, and biogenic methane from dissociation of sub-seafloor clathrates[3,6,11-13]. Early Toarcian elevated atmospheric pCO_2 likely induced climatic and environmental change[5,12,14-16] by accelerating the global hydrological cycle and increasing silicate weathering, thereby increasing delivery of riverine nutrients to the oceans and potentially also to large inland lakes[17]. In the marine realm, the consequential increase in primary productivity and carbon flux to the sea floor is credited with enhancing the burial of planktonic material in relatively deep continental-margin sites, whereas in shallower water semi-restricted marine basins, chemical and physical water-column stratification likely aided the burial of organic matter[17]. Particularly in northern Europe, the evidence points to regional to global development of anoxic/euxinic (sulphide-rich) bottom waters that strongly affected palaeoceanographic conditions and marine ecosystems[15,17,18]. Globally significant burial of ^{13}C-depleted photosynthetically derived organic matter commonly produced an overarching positive carbon-isotope excursion (CIE) interrupted by the

55 characteristic abrupt negative shift that invariably characterizes the T-OAE (early
56 Toarcian *tenuicostatum–falciferum* ammonite biozones)[1,2,18].

57 Marine records of the T-OAE, based on the presence of apparently coeval
58 organic-rich shales, have now been identified from many outcrops in both the
59 northern and southern hemispheres[2,5], but climatic and environmental change on the
60 continents is still poorly understood. Intriguingly, however, sedimentary archives
61 from continental interiors in China (e.g. the Tarim, Ordos and Sichuan Basins) are
62 consistently marked by the occurrence of organic-rich black shales that are latest
63 Early Jurassic in age[19-21]. This stratigraphic evidence suggests that major inland lakes
64 potentially formed or expanded contemporaneously with the T-OAE. Here, we (1)
65 determine the precise age of the upper Lower Jurassic lacustrine organic-rich black
66 shales in the Sichuan Basin; (2) determine their depositional context; and (3) explore
67 the possible relevance of major lake formation as an additional sink for carbon in the
68 context of the major disturbance in the early Toarcian exogenic carbon cycle.

69

70 AGE AND STRATIGRAPHY

71 The present-day topographic Sichuan Basin covers a total area of ~230,000 km^2 (ref.
72 22), almost three times the size of Lake Superior (82,100 km^2), the most extensive
73 modern freshwater lake in the world. The Early Jurassic Sichuan Basin (and the
74 palaeo-Sichuan lake system) is thought to have been even larger than its present-day
75 confines[23] (Fig. 1). Two cores, named A and B, (Fig. 1) were taken from the more
76 proximal, northwestern part of the Sichuan Basin, each penetrating the entire
77 Da'anzhai Member, which is ~50–70 m in thickness here. The Da'anzhai Member in
78 both successions exhibits alternating beds of fossiliferous carbonate and a spectrum of
79 mudrocks from clay-rich marl to laminated black shale (Fig. 2). Diverse freshwater

bivalves, ostracods, gastropods and conchostracans in the fossiliferous carbonate beds and mudstone beds confirm these sediments to be lacustrine deposits[24]. The freshwater ostracod faunal assemblages, which include *Darwinula* spp. and *Metacypris unibulla,* suggest a late Early Jurassic age[25].

Here, palynostratigraphy, Re-Os chronology and chemostratigraphy are utilized to constrain further the depositional age of the Da'anzhai Member (see Methodology-section [2] for more detailed discussion). Re-Os radio-isotopic dating of 16 samples from two combined intervals of the Da'anzhai lacustrine black shale (Core A) provides a well-constrained single isochron of 180±3.2 Ma (Fig. 3; Supplementary Information Fig. S1), constraining the Da'anzhai Member to be of Toarcian age[26]. The palynomorph assemblages obtained from the studied cores closely resemble floras from lower Toarcian marine successions in northern Europe and Australia, further suggesting a similar depositional age for the lacustrine Da'anzhai Member (see Methodology-section [2]). The observed parallel signature in $\delta^{13}C_{TOC}$ (Cores A and B) and $\delta^{13}C_{n\text{-alkane}}$ (Core A) in the main phase of the Da'anzhai Member (above 2698 m) (Figs 2 and 3) likely reflects a true perturbation of the global exogenic carbon cycle (see Methodology-section). It is similar in shape and magnitude to what is characteristically observed in early Toarcian marine calcite and compound-specific marine and terrestrial organic- matter records from Europe and elsewhere spanning the T-OAE[4,8–10] (Fig. 3).

The combined macro- and microfossil biostratigraphy, palynostratigraphy, Re-Os chronology and chemostratigraphy uniquely constrain the formation of the Da'anzhai Member to be time-equivalent with the T-OAE.

DEPOSITIONAL ENVIRONMENT OF THE DA'ANZHAI MEMBER

105 Terrestrial (fluvial/deltaic and soil) deposits of the Ma'anshan Member in the mid-
106 Early Jurassic Sichuan Basin pass up-section into the lacustrine facies of the
107 Da'anzhai Member. Chemostratigraphic correlation between the more distal Core A
108 and the more proximal Core B, based on elevated total organic carbon (TOC) and HI
109 and the observed $\delta^{13}C_{TOC}$ negative CIE, suggests a diachronous base of the Da'anzhai
110 Member, as defined by the presence of characteristic lacustrine facies lying
111 stratigraphically above palaeosols (Fig. 2). The lower half of the Da'anzhai Member
112 in Core A is marked by abundant fossiliferous limestone, primarily consisting of
113 bivalve and ostracod shell fragments, alternating with more clay-rich sediments. This
114 interval is also marked by generally low TOC (~1%) and HI values (~150 mg C/g
115 TOC), suggesting a near-shore depositional environment with low aquatic organic
116 matter productivity and/or preservation. The abrupt transition from palaeosol to
117 fossiliferous limestone at ~2714.85 m, followed by the transition to laminated
118 organic-rich black shale at ~2693.40 m in the more distal Core A, and the coeval
119 transition from palaeosol to laminated organic-rich black shale at ~3156.34 m in Core
120 B (Fig. 2), suggests the rapid expansion and deepening of the lake, with decreased
121 macrofossil carbonate supply (Fig. 4). Macrofossils in the regularly occurring
122 limestone beds show variable orientation and degrees of fragmentation and,
123 depending on the stratigraphic horizon, are in life position, or were subjected to local
124 transport and re-deposition. The interbedded marls and black shales are interpreted as
125 representing quieter water sedimentation and/or sedimentation inimical to benthic life.
126 The fossil assemblages from both cores signify a predominantly non-marine
127 depositional environment, with the occurrence of the freshwater bivalve genus
128 *Margaritifera*[24], lacustrine ostrocods, and the freshwater/brackish alga *Botryococcus*
129 (Supplementary Information). However, some intervals in Core A (2684.49 m to

2695.80 m and 2702.49 m to 2710.73 m) contain *in situ* marine palynomorphs such as the acritarch *Veryhachium collectum* and the prasinophyte *Halosphaeropsis liassica* (Fig. 2, Supplementary Information). These occurrences suggest marine incursions into the basin. Significantly, the oldest sediments of the lacustrine Da'anzhai Member studied in Core A are devoid of acritarchs (Fig. 2; Supplementary Information), indicating that the lake had already developed before any potential marine incursion took place. Furthermore, the relative abundance of acritarchs in the samples studied shows no positive correlation with TOC or (pyritic) sulphur abundance (Figs 2 and 3), indicating that deposition of the most organic-rich sediments and the supply of sulphate was unrelated to a potential marine connection. Sedimentary facies in Europe and elsewhere indicate that the early Toarcian witnessed a significant marine transgression, culminating in the *falciferum* ammonite biozone[27,28]. Although the Early Jurassic Sichuan Basin was surrounded by compressional mountain ranges in the north, east and west, the palaeo-Sichuan lake system likely formed close to sea level and the basin could, therefore, have been temporarily connected to the ocean to the south (Fig. 1 and references herein, Fig. 4). Overall, however, the abundance of freshwater fossils and palynomorphs, combined with a highly elevated radiogenic initial $^{187}Os/^{188}Os$ composition of ~1.29, significantly higher than Early Jurassic Toarcian open marine $Os_{initial}$ values of 0.4−0.8 recorded from Europe[29] (Supplementary Information), points to a dominantly lacustrine environment during the deposition of the Da'anzhai Member. This interpretation is further supported by the presence of tetracyclic polyprenoids (TPP) (typically sourced from freshwater algae; Supplementary Information Fig. S5), the near absence of C_{30} steranes (typically sourced from marine algae; Supplementary Information Fig. S6) and high hopane over sterane biomarker ratios throughout Core A[30,31] (Supplementary Information).

Previous study on a section from Bornholm, Denmark suggested a sharp increase of atmospheric pCO_2 reconstructed from terrestrial leaf stomatal density at the onset of the negative CIE[12]. The increased occurrence of *Classopollis* in tetrads (relative to single specimens; Fig. 2) observed during the negative CIE interval suggests stressed environmental conditions on land during the T-OAE, likely in response to enhanced atmospheric pCO_2 and greenhouse-gas-induced climatic warming[12,14,18,32,33].

The Toarcian mid-palaeolatitude setting and geomorphology of the palaeo-Sichuan Basin, with surrounding high mountain ranges[21], may have made the basin susceptible to an enhanced monsoonal system and increased hydrological cycle with high amounts of run-off, particularly when warm shallow transgressive seas approached (Fig. 4) (cf. the modern South Asian monsoon[34]). The formation or strong expansion of the palaeo-lake system in the early Toarcian Sichuan Basin, with the deposition of the Da'anzhai Member lacustrine black shales with elevated TOC (of up to ~3.3%) and HI (of up to 450 mg HC/g TOC) levels, suggests increased aquatic primary productivity due to increased continental weathering and accelerated riverine nutrient supply. Significantly, based on all the stratigraphic data herein (Fig. 3), the level of maximum TOC enrichment in the Da'anzhai Member developed coevally with the most organic-rich black shale in marine sections from Yorkshire, UK (Fig. 3), consistent with a fundamental global climatic control on the introduction of nutrients into aquatic environments, even though the quantity and type of organic matter deposited and preserved may have been different.

Elevated sulphur concentrations in the most organic-rich sections of laminated black shale of the Da'anzhai Member in Core A (Fig. 3; Supplementary Information), coincide with the occurrence of small (<5 μm diameter) and also larger pyrite

framboids (Supplementary Information Fig. S11). The source of sulphur is, however, as yet uncertain, but lake sulphate could have originated from the weathering of the Lower–Middle Triassic evaporites in the hinterland[22]. Although the larger pyrite framboids could have formed diagenetically in sulphide-rich sedimentary pore-waters, the smaller framboids (<5 μm) likely formed by sulphate reduction in the water column, as typically happens under euxinic conditions[35]. The stratigraphic intervals with high (pyritic) sulphur concentrations coincide with levels of elevated sedimentary molybdenum enrichment (with Mo >20 ppm; Fig. 3). In oxic conditions, Mo exists as soluble molybdate (MoO_4^{2-}) that adsorbs onto Mn-oxides and only slowly precipitates. In sulphidic (euxinic) waters, however, molybdate dissociates into thiomolybdate anions, which are rapidly reduced to highly reactive Mo(IV)-sulphides that precipitate out of solution, leading to sedimentary Mo enrichment[36]. Furthermore, water-column stratification, which is a likely prerequisite for sustained euxinia, is also supported by elevated levels of gammacerane in the black-shale interval of Core A (Fig. 2; Supplementary Information). Gammacerane is a biomarker derived from tetrahymanol that forms in abundance under conditions of high bacterial productivity within stratified water columns, commonly in lakes or isolated marine basins[37]. The combined geochemical and mineralogical data suggest the development of a physically or chemically stratified water column during laminated black-shale formation in the palaeo-Sichuan Lake, even in relatively proximal depositional settings.

LACUSTRINE CARBON BURIAL AND THE TOARCIAN CARBON CYCLE

The early Toarcian negative CIE has been widely attributed to the release of ^{13}C-depleted volcanogenic CO_2 and/or methane from either thermal metamorphism of

205 Gondwanan coals or the dissociation of sub-sea-floor gas hydrates, also resulting in
206 enhanced early Toarcian atmospheric pCO_2 levels[3,11,12,15]. The typical early Toarcian
207 $\delta^{13}C$ pattern, with a stepped negative shift interrupting an overarching positive
208 excursion, has been observed in marine and terrestrial organic matter and shallow-
209 water platform and deep-water pelagic carbonates and manifestly affected the entire
210 ocean–atmosphere system[3,5,6,8]. The overall positive shift is attributed to globally
211 accelerated organic-carbon burial whereas the superimposed stepped negative shift
212 suggests that the release of isotopically light carbon took place in pulses that have
213 been attributed to astronomical forcing of the global carbon cycle[6]. Astronomical
214 interpretation of periodic fluctuations in chemical and physical proxy records estimate
215 the duration of the early Toarcian negative CIE at 300−900 kyr[6,38–40].

216 In the early Toarcian Sichuan Basin, the laminated black-shale interval in both
217 cores is marked by elevated HI and TOC values (with HI up to 450 mg HC/g TOC
218 and TOC up to 3.3% in the more distal Core A), likely reflecting increased algal
219 primary productivity, in addition to a background supply of terrestrial organic matter,
220 during the interval with the lowest carbon-isotope values of the negative CIE. This
221 chemostratigraphic pattern is very similar to that developed in marine sections from
222 northern Europe, where sedimentary TOC-levels can locally reach ~20%. Box-model
223 studies for the early Toarcian carbon cycle suggest that the release of ~9000 Gt
224 carbon from methane clathrates (with $\delta^{13}C$ of ~ -60‰) or ~25,000 Gt carbon as
225 thermogenic methane (with $\delta^{13}C$ of ~ -35‰), is required to generate a negative $\delta^{13}C$
226 excursion compatible with the mean change in bulk carbonate of 4–6‰, and which
227 would have caused an increase in atmospheric pCO_2 of ~1000 ppm[7,8,15,41]. Excess
228 atmospheric CO_2 is assumed to have been sequestered both by enhanced weathering
229 of Ca-Mg silicates due to greenhouse warming, and by massive burial of organic

carbon in marine dysoxic, anoxic and euxinic depositional environments[17]. These combined processes would have dictated the pattern of $\delta^{13}C$ recovery, but the total amount of ^{13}C-depleted carbon released may have been even larger than modelled because enhanced ^{12}C-enriched carbon burial would have acted as a mechanism to potentially increase ocean-atmosphere $\delta^{13}C$ during the onset of the T-OAE, even though the resultant summed effect was to move values in the opposite direction.

Sequestration of carbon in marine basins is generally considered to have been a major driver behind $\delta^{13}C$ recovery. The sheer size of the latest Early Jurassic continental basins, and the expansion of this major lake in response to early Toarcian environmental change provide, however, an additional, and significant, sink for carbon. The Da'anzhai Member lacustrine black shale formed over 70,000 km^2 in the palaeo-Sichuan Basin, with an average thickness of 60−120 m and 0.8−3.5% TOC; lacustrine marl and carbonate accumulated coevally over large parts of the remaining 160,000 km^2 of the basin[42]. Applying the average of these parameters, it is estimated that ~460 Gt of organic carbon and ~1200 Gt of inorganic carbon was extracted from the global ocean–atmosphere system and sequestered in the palaeo-Sichuan lake during deposition of the lower Toarcian Da'anzhai Member black shales alone (Supplementary Information). This figure is, however, a conservative estimate because original sedimentary TOC values may have been even higher considering the present-day maturity of the rock. Also, TOC values in the deepest, most central part of the basin may have been more elevated than in the more proximal cores studied herein. Enhanced continental inorganic-carbon burial would not affect the isotopic composition of exogenic carbon reservoirs, but the burial of isotopically depleted organic carbon would shift the carbon-isotope composition of the global exogenic carbon cycle to more positive values. Assuming the (pulsed) release of 9,000 Gt of

carbon from methane clathrates (with a $\delta^{13}C$ of ~ -60‰) or 25,000 Gt as thermogenic methane (with a $\delta^{13}C$ of ~ -35‰) to explain the observed step-wise negative shift in $\delta^{13}C$ (-5‰; from 1‰ to -4‰) during the T-OAE[41], and assuming global carbon sequestration largely by organic-matter burial (with a $\delta^{13}C$ of -25‰) to explain the observed recovery in global $\delta^{13}C$, a simple mass-balance model indicates that early Toarcian organic carbon burial in the black shale of the palaeo-Sichuan Basin alone sequestered 1.3−2.2% of the total amount sequestered to recover from the $\delta^{13}C$ negative shift during the T-OAE negative CIE (Supplementary Information). The present-day global lake surface area is about ~0.69% of the surface area of the global ocean; lakes, however, account for ~10% of the global carbon drawdown and burial[43]. The palaeo-Sichuan lake alone covered over ~230,000 km^2, which is ~10% of the present-day global lake surface, but it was responsible for, at least, 1.3–2.2% of the global organic carbon burial flux. The generation of massive sinks of carbon in the early Toarcian continental interiors by the formation and/or expansion of major lakes and subsequent sequestration of carbon, in addition to marine carbon burial, potentially significantly impacts the nature and duration of the observed exogenic carbon-cycle perturbation. If the carbon sink of the Sichuan Basin black shale had not formed, and with the assumption of constant climatic/environmental parameters affecting the rate of carbon drawdown, the recovery from the $\delta^{13}C$ negative shift would have required an additional ~4,000–20,000 yr of global marine carbon drawdown (Supplementary Information). In addition, massive burial of inorganic carbon in the Sichuan Basin, extracted from the ocean–atmosphere system, would have significantly lowered atmospheric pCO_2, which likely further shortened the Early Toarcian climatic perturbation. Given that several other lacustrine basins, for example, the Tarim and Ordos Basins in northwestern and central northern China

(Fig. 1) also appear to have developed in the late Early Jurassic with the deposition of organic-rich sediments[19,20], these figures are undoubtedly minima.

These results suggest an as-yet-unexplored, negative feedback in the global exogenic carbon cycle during oceanic anoxic events. Climatic warming induced by addition of greenhouse gases to the atmosphere, and an associated increase in hydrological cycling, allowed for the formation of major lake systems in continental settings, where enhanced fluvial nutrient supply with increased productivity and preservation could have lead to major carbon sequestration. Together with widespread burial of organic matter in the marine realm, the lacustrine carbon sink would have reduced atmospheric pCO_2, allowed rebound of the global $\delta^{13}C$ signal, and cooled global climate through an inverse greenhouse effect[18].

References

1. Jenkyns, H. C. The early Toarcian and Cenomanian-Turonian anoxic events in Europe: comparisons and contrasts. *Geol. Rundsch.* **74**, 505–518 (1985).
2. Jenkyns, H. C. The early Toarcian (Jurassic) anoxic event: stratigraphic, sedimentary, and geochemical evidence. *Am. J. Sci.* **288**, 101–151 (1988).
3. Hesselbo, S. P. *et al.* Massive dissociation of gas hydrate during a Jurassic oceanic anoxic event. *Nature* **406**, 392–395 (2000).
4. Sælen, G., Tyson, R.V., Telnæs, N. & Talbot, M.R. Constracting watermass conditions during deposition of the Whitby Mudstone (Lower Jurassic) and Kimmeridge Clay (Upper Jurassic) formations, UK. *Palaeogeogr. Palaeoclimatol. Palaeoecol.* **163**, 163–196 (2000).
5. Jenkyns, H. C., Jones, C. E., Grocke, D. R., Hesselbo, S. P. & Parkinson, D. N. Chemostratigraphy of the Jurassic System: applications, limitations and implications for palaeoceanography. *J. Geol. Soc. London* **159**, 351–378 (2002).
6. Kemp, D. B., Coe, A. L., Cohen, A. S. & Schwark, L. Astronomical pacing of methane release in the Early Jurassic period. *Nature* **437**, 396–399 (2005).
7. Hesselbo, S. P., Jenkyns, H. C., Duarte, L. V. & Oliveira, L. C. V. Carbon-isotope record of the Early Jurassic (Toarcian) Oceanic Anoxic Event from fossil wood and marine carbonate (Lusitanian Basin, Portugal). *Earth Planet. Sci. Lett.* **253**, 455–470 (2007).
8. Hermoso, M., Le Callonnec, L., Minoletti, F., Renard, M. & Hesselbo, S. P. Expression of the Early Toarcian negative carbon-isotope excursion in separated carbonate microfractions (Jurassic, Paris Basin). *Earth Planet. Sci. Lett.* **277**, 194–203 (2009).
9. French, K.L., Sepúlveda, J., Trabucho-Alexandre, J., Gröcke, D.R. & Summons, R.E. Organic geochemistry of the early Toarcian oceanic anoxic event in Hawsker Bottoms, Yorkshire, England. *Earth Planet. Sci. Lett.* **390**, 116–127 (2014).

10. Suan, G., van de Schootbrugge, B., Adatte, T., Fiebig, J. & Oschmann, W. Calibrating the magnitude of the Toarcian carbon cycle perturbation. *Paleoceanography* **30**, 495–509 (2015).
11. Duncan, R. A., Hooper, P. R., Rehacek, J., Marsh, J. S. & Duncan, A. R. The timing and duration of the Karoo igneous event, southern Gondwana. *J. Geophys. Res.-Sol. Ea.* **102**, 18127–18138 (1997).
12. McElwain, J. C., Wade-Murphy, J. & Hesselbo, S. P. Changes in carbon dioxide during an oceanic anoxic event linked to intrusion into Gondwana coals. *Nature* **435**, 479–482 (2005).
13. Svensen, H. *et al.* Hydrothermal venting of greenhouse gases triggering Early Jurassic global warming. *Earth Planet. Sci. Lett.* **256**, 554–566 (2007).
14. Dera, G. *et al.* Climatic ups and downs in a disturbed Jurassic world. *Geology* **39** 215–218 (2011).
15. Ullmann, C. V., Thibault, N., Ruhl, M., Hesselbo, S. P. & Korte, C. Effect of a Jurassic oceanic anoxic event on belemnite ecology and evolution. *Proc. Natl. Acad. Sci. USA* **111**, 10073–10076 (2014).
16. Brazier, J. M. *et al.* Calcium isotope evidence for dramatic increase of continental weathering during the Toarcian oceanic anoxic event (Early Jurassic). *Earth Planet. Sci. Lett.* **411**, 164–176 (2015).
17. Jenkyns, H. C. Geochemistry of oceanic anoxic events. *Geochem. Geophy. Geosy.* **11**, Q03004, doi: 10.1029/2009gc002788 (2010).
18. Jenkyns, H. C. Evidence for rapid climate change in the Mesozoic-Palaeogene greenhouse world. *Philos. T. R. Soc. A* **361**, 1885–1916 (2003).
19. Huang, K. *et al*. Sedimentary environments and palaeoclimate of the Triassic and Jurassic in Kuqa River area, Xinjinag (in Chinese with English abstract). *Journal of Palaeogeography* **5**, 197–208 (2003).
20. Yang, Y., Li, W. & Ma, L. Tectonic and stratigraphic controls of hydrocarbon systems in the Ordos basin: A multicycle cratonic basin in central China. *AAPG Bulletin* **89**, 255–269 (2005).
21. He, F. & Zhu, T. Favorable targets of breakthrough and built-up of shale gas in continental facies in Lower Jurassic, Sichuan Basin (in Chinese with English abstract). *Petroleum Geology & Experiment* **34**, 246–251 (2012).
22. Cai, C., Worden, R. H., Bottrell, S. H., Wang, L. & Yang, C. Thermochemical sulphate reduction and the generation of hydrogen sulphide and thiols (mercaptans) in Triassic carbonate reservoirs from the Sichuan Basin, China. *Chem. Geol.* **202**, 39–57 (2003).
23. Guo, T., Li, Y. & Wei, Z. Reservoir-forming conditions of shale gas in Ziliujing Formation of Yuanba Area in Sichuan Basin (in Chinese with English abstract). *Natural Gas Geoscience* **22**, 1–7 (2011).
24. Wang, Y. *et al*. *The terrestrial Triassic and Jurassic Systems in the Sichuan Basin, China*. (University of Science & Technology of China Press, 2010).
25. Wei, M. in *Continental Mesozoic stratigraphy and paleontology in the Sichuan Basin* (in Chinese) 346–363 (People's Publishing House of Sichuan, 1982).
26. Ogg, J. G. & Hinnov, L.A. in *The Geologic Time Scale 2012* Vol. 2 (eds Gradstein, F.M.; Ogg, J.G.; Schmitz, M.D. & Ogg, G.M.) Ch. 26, 731–791 (Elsevier, 2012).
27. Hallam, A. A revised sea-level curve for the Early Jurassic. *J. Geol. Soc. London* **138**, 735–743 (1981).
28. Suan, G. *et al.* Polar record of Early Jurassic massive carbon injection. *Earth Planet. Sci. Lett.* **312**, 102–113 (2011).
29. Percival, L.M.E., Cohen, A.S., Davies, M.K., Dickson, A.J., Hesselbo, S.P., Jenkyns, H.C., Leng, M.J., Mather, T.A., Storm, M.S. & Xu, W. Osmium isotope evidence for two pulses of increased continental weathering linked to Early Jurassic volcanism and climate change. *Geology* doi: 10.1130/G37997.1 (2016).

30. Moldowan, J. M., Seifert, W. K. & Gallegos, E. J. Relationship between petroleum composition and depositional environment of petroleum source rocks. *AAPG Bulletin* **69**, 1255–1268 (1985).
31. Holba, A. G., Tegelaar, E., Ellis, L., Singletary, M. S. & Albrecht, P. Tetracyclic polyprenoids: Indicators of freshwater (lacustrine) algal input. *Geology* **28**, 251–254 (2000).
32. Vakhrameyev, V. A. Pollen *Classopollis*: indicator of Jurassic and Cretaceous climate. *Paleobotanist* **28-29**, 301–307 (1981).
33. Kürschner, W. M., Batenburg, S. J. & Mander, L. Aberrant *Classopollis* pollen reveals evidence for unreduced (2n) pollen in the conifer family Cheirolepidiaceae during the Triassic–Jurassic transition. *Proc. Biol. Sci.* **280**, 20131708 (2013).
34. Boos, W.R. & Kuang, Z. Dominant control of the South Asian monsoon by orographic insulation versus plateau heating. *Nature* **463**, 218–222 (2010).
35. Wilkin, R. T. & Barnes, H. L. Pyrite formation by reactions of iron monosulfides with dissolved inorganic and organic sulfur species. *Geochim. Cosmochim. Acta* **60**, 4167–4179 (1996).
36. Dahl, T. W. *et al.* Tracing euxinia by molybdenum concentrations in sediments using handheld X-ray fluorescence spectroscopy (HHXRF). *Chem. Geol.* **360**, 241–251 (2013).
37. Sinninghe Damsté, J. S. *et al.* Evidence for Gammacerane as an indicator of water column stratification. *Geochim. Cosmochim. Acta* **59**, 1895–1900 (1995).
38. Kemp, D. B., Coe, A. L., Cohen, A. S. & Weedon, G. P. Astronomical forcing and chronology of the early Toarcian (Early Jurassic) oceanic anoxic event in Yorkshire, UK. *Paleoceanography* **26**, PA4210, doi:10.1029/2011pa002122 (2011).
39. Suan, G. *et al.* Duration of the Early Toarcian carbon isotope excursion deduced from spectral analysis: Consequence for its possible causes. *Earth Planet. Sci. Lett.* **267**, 666–679 (2008).
40. Boulila, S. *et al.* Astronomical calibration of the Toarcian Stage: Implications for sequence stratigraphy and duration of the early Toarcian OAE. *Earth Planet. Sci. Lett.* **386**, 98–111 (2014).
41. Beerling, D. J. & Brentnall, S.J. Numerical evaluation of mechanisms driving Early Jurassic changes in global carbon cycling. *Geology* **35**, 247–250 (2007).
42. Zou, C. in *Unconventional Petroleum Geology*. Ch. 3, 61–109 (Petroleum Industry Press, 2013).
43. Dean, W.E. & Gorham, E. Magnitude and significance of carbon burial in lakes, reservoirs, and peatlands. *Geology* **26**, 535–538 (1998).
44. Cohen, A. S., Coe, A. L., Harding, S. M. & Schwark, L. Osmium isotope evidence for the regulation of atmospheric CO_2 by continental weathering. *Geology* **32**, 157–160 (2004).

Acknowledgements Shell International Exploration & Production B.V. is acknowledged for financial support for this study. D.S. acknowledges the Total endowment fund. We thank Shell Global Solutions B.V., Shell China Exploration & Production Co. Ltd, and PetroChina Southwest Oil and Gasfield Company for approval to publish this study. Tai-Ran Jiang, Malcolm Dransfield and Xue-Yan Li (Shell China Exploration and Production Co. Ltd.), Olaf Podlaha, Sander van den

Boorn (Shell Global Solutions International B.V.), Qinggao Zeng and Zhiping Tang (PetroChina Southwest Oil and Gasfield Company) and Bruce Levell (University of Oxford) are acknowledged for discussions and reviews of earlier versions of the manuscript and for providing sample materials. We also thank reviewers David Kemp and Guillaume Suan and an anonymous reviewer for comments and suggestions that have greatly improved this manuscript. CGG Robertson and Shell are acknowledged for providing the palaeogeographic reconstruction used in Figure 1. J.B.R. publishes with the approval of the Executive Director, British Geological Survey (NERC). This paper is also a contribution to UNESCO-IUGS IGCP Project 632.

Author contribution statement

W. X., M.R., H.C.J. and S.P.H. designed the project. W.X. and M.R. performed core description and sampling. W.X., M.R., J.B.R., D.S., J.W.H.W. and B.D.A.N. performed geochemical and palynological analyses. All authors contributed to data analysis and interpretation and writing and/or refinement of the manuscript.

Additional information

Supplementary information is available in the online version of the paper. Reprints and permissions information is available online at www.nature.com/reprints. Correspondence and requests for materials should be addressed to W. X.

Competing financial interests

The authors declare no competing financial interests.

Figure captions

Figure 1 Size and location of the palaeo-Sichuan lake at 179 Ma. The map on the left shows a regional tectonic plate reconstruction at 179 Ma (edited from a map provided by CGG Robertson and Shell), with positions of the latest Early Jurassic lacustrine Sichuan, Tarim and Ordos Basins marked[21,23,42]. The map on the right illustrates the location of the two cores studied within the Sichuan Basin; relative variations in lake depth are illustrated in blue, with the darker shade representing deeper water areas; the green brickwork represents fossiliferous limestone and the yellow dotted ornaments represent deltaic deposits; palaeo-mountain ranges are marked in brown and thickness of the Da'anzhai Member is indicated by the isopachs.

Figure 2 Stratigraphic correlation of cores A and B and palaeoenvironmental proxies in the Sichuan Basin (China). Stratigraphic changes in lithology from each core are illustrated by Ca concentrations (from XRF measurements on the core-slabs) superimposed on the combined core photos, with light colours representing limestone and dark colours representing shale. $\delta^{13}C_{TOC}$ from both cores are plotted in red squares and the 3-point moving averages are plotted in thick red lines. $\delta^{13}C_{n\text{-alkane}}$ data from different chain-lengths are plotted in diamonds of different colours, as illustrated in the legend. Error bars on $\delta^{13}C_{n\text{-alkane}}$ data reflect the 1σ standard deviation of replicates. TOC and HI values from Rock-Eval pyrolysis are plotted for both cores in black and dark blue squares, respectively (note similar pattern of TOC enrichment). The Gammacerane Index values (Gammacerane/C_{30} Hopane) are plotted in yellow diamonds. Marine acritarch percentages (%) are plotted in the larger blue squares with light blue shades. Ratios of *Classopollis sp.* tetrads *vs* single grains are plotted in black squares.

Figure 3 Geochemical comparison between the lacustrine Da'anzhai Member (Sichuan Basin, China) and the lower Toarcian marine succession from

Yorkshire (UK). Re-Os (Rhenium-Osmium) isochrons from both Yorkshire[44] and the Da'anzhai Member (Sichuan Basin; this study) are plotted with short dashed lines, indicating the depths of samples that produced the Re-Os isochrons. The Re-Os isochron from the upper Lower Jurassic lacustrine Da'anzhai Member (Core A) gives an age of 180.3±3.2 Ma, and the Lower Toarcian marine Jet Rock (Yorkshire) gives a Re-Os isochron age of 178.2±5.6 Ma[44]. The two successions are correlated based on $\delta^{13}C_{TOC}$ and $\delta^{13}C_{n\text{-alkane}}$ from the Da'anzhai Member, and $\delta^{13}C_{TOC}$[6,44], $\delta^{13}C_{n\text{-alkane}}$[9] and $\delta^{13}C_{phytane}$[4] from Yorkshire. S and Mo concentrations (from XRF measurements) and TOC (from Rock Eval pyrolysis) on Core A are plotted in yellow lines, blue diamonds and black lines with dark grey shades, respectively. TOC and S records from Yorkshire[38] are plotted in yellow lines and black lines with dark grey shades, respectively. A conservatively estimated ~460 Gt organic carbon was buried in the palaeo-Sichuan lake system during the T-OAE.

Figure 4 Model for the formation of lacustrine conditions in the Sichuan Basin. On the right are idealized $\delta^{13}C$ records across the T-OAE, with the stratigraphic intervals marked with grey shading representing the different phases in lake evolution. Phase A: the continental Sichuan Basin was marked by fluvial and terrestrial sedimentary deposition pre-T-OAE negative CIE, with possibly geographically restricted lacustrine conditions in the central part of the basin. Phase B: early Toarcian temperature and sea-level rise increased evaporation from the approaching marine waters, enhancing the hydrological cycle and promoting precipitation in the continental interior of the Sichuan Basin, which resulted in the formation or strong expansion of the palaeo-Sichuan lake. Phase C: continuing late Early Toarcian eustatic sea-level rise allowed for occasional marine incursions into the dominantly lacustrine palaeo-Sichuan basin. Phase D: eustatic sea-level fall in the

494 latest Early Toarcian initiated the return to fully lacustrine conditions and maximum
495 marine and lacustrine organic carbon burial. Phase E: global recovery from the Early
496 Toarcian climatic perturbation, with associated reduction in global temperature and
497 cessation of enhanced hydrological cycling, initiated the return to a terrestrial and
498 fluvial depositional environment in the Sichuan Basin.
499
500
501 METHODOLOGY
502 [1] GEOLOGICAL SETTING OF THE SICHUAN BASIN
503 The Sichuan Basin formed on the western part of the Yangtze Platform, in
504 which sedimentation commenced with the Neoproterozoic Sinian Sequence (850–570
505 Ma)[45]. Shallow-marine carbonates formed from the Tonian to the Middle Triassic,
506 with occasional epeirogenic events, e.g. widespread basalt emplacement due to
507 extension of the western margin of the Yangtze Platform, in the Late Palaeozoic[45].
508 Sedimentation switched from marine to continental in the Middle to Late Triassic
509 with Indosinian tectonic uplift due to closure of the Palaeotethys and collision of the
510 North and South China cratonic blocks[22]. Siliciclastic sediments were deposited as
511 alluvial fans and lakeshore–deltaic plain facies in the Early Jurassic, particularly
512 along the southern front of the Longmen and Micang-Daba mountain ranges at the
513 northwestern and northern margins of the Sichuan Basin[21,23,42,45] (Fig. 1).
514 Continental/fluvial deposits and green/red pedogenic horizons with soil carbonate
515 nodules mark the Ma'anshan Member (middle Ziliujing Formation) and underlie the
516 lacustrine facies of the upper Lower Jurassic Da'anzhai Member (uppermost Ziliujing
517 Formation). The Da'anzhai Member represents the development of dominantly
518 lacustrine conditions and the formation of a major lake. Lacustrine conditions may,

519 however, have persisted through most of the Early Jurassic in the most central and
520 deepest part of the basin, although their onset and termination are still poorly dated[46].
521
522 [2] AGE MODEL
523 Re-Os radiometric dating on 16 samples from two combined intervals of the
524 Da'anzhai lacustrine black shale (Core A) shows a well-constrained single isochron of
525 180.3±3.2 Ma (Fig. 3; Supplementary Information Fig. S1), constraining the
526 Da'anzhai Member to the Toarcian, following the Jurassic timescale of Ogg and
527 Hinnov (2012)[26]. A Re-Os isochron for the organic-rich marine mudrock from the
528 *falciferum* ammonite subzone in Yorkshire (UK) suggests a depositional age of
529 178.2±5.6 Ma[44]. The age obtained here for the lacustrine Da'anzhai Member in the
530 Sichuan Basin is in agreement, within uncertainty, with the marine realm early
531 Toarcian Re-Os isochron-based age (Fig. 3; Supplementary Information Fig. S2).
532 The palynomorph assamblages of the lacustrine Da'anzhai Member, with the
533 superabundance of the pollen *Classopollis* sp. (and the absence of *Callialasporites*
534 spp.), the occurrence of the spore *Ischyosporites vaerigatus*, the acritarch
535 *Veryhachium collectum*, multi-specimen clumps of the prasinophyte *Halosphaeropsis*
536 *liassica* and the rare occurrence of the dinoflagellate cyst ?*Skuadinium* sp., are
537 comparable to floras from lower Toarcian marine successions in northern Europe and
538 Australia, indicating that the successions studied here are of similar age
539 (Supplementary Information Fig. S4 shows a range chart with selected palynomorph
540 occurrence). The superabundance of the thermophylic pollen genus *Classopollis* and
541 the occurrence of the opportunistic prasinophyte species *Halosphaeropsis liassica,*
542 thought to have thrived in environmentally stressed conditions and normally

543 occurring in multi-specimen clumps, are especially typical of the T-OAE
544 (Supplementary Information)[47–50].

545 Furthermore, $\delta^{13}C_{TOC}$ analyses of Core A reveal <3‰ fluctuations in the basal
546 15 m of the Da'anzhai Member, followed by a transient ~4‰ negative excursion (Fig.
547 2). The base of Core B is interpreted to be stratigraphically younger than Core A
548 based on carbon-isotope correlation, and similarly shows a ~4‰ negative excursion
549 in $\delta^{13}C_{TOC}$ (Fig. 2), followed by a full positive return to initial base values. The two
550 cores combined illustrate the complete negative CIE, which is similar in shape and
551 magnitude to that observed in marine records of the T-OAE (Fig. 3)[6,44]. Compound-
552 specific long-chain *n*-alkane (C_{23}–C_{33}) $\delta^{13}C$ analyses of Core A also show a distinct
553 ~4‰ negative excursion, similar in magnitude to the bulk organic-matter $\delta^{13}C_{TOC}$
554 from the same stratigraphic interval (Figs 2 and 3). Long-chain *n*-alkanes in
555 sedimentary organic matter are typically sourced from terrestrial higher plants or
556 freshwater algae[51] whose isotopic compositions are commonly indistinguishable
557 because lake-water dissolved inorganic carbon (DIC) is isotopically in equilibrium
558 with the atmosphere[52]. Consequently, the observed shift in $\delta^{13}C_{n\text{-alkanes}}$ directly reflects
559 changes in the carbon-isotope composition of the atmosphere (and lake-water DIC)
560 during the early Toarcian global carbon-cycle perturbation. The odd-over-even
561 predominance in the long-chain (C_{23}−C_{33}) *n*-alkane distribution, typical for terrestrial
562 higher plant leaf waxes or freshwater algal-sourced sedimentary organic matter[51] is,
563 however, not observed from Core A (with a Carbon Preference Index of ~1), probably
564 due to its relatively elevated thermal maturity[53]. The ~2–3‰ carbon-isotope
565 fluctuations in $\delta^{13}C_{TOC}$ in the lower Da'anzhai Member of Core A (2702–2715m in
566 the core) are, however, not repeated in the $\delta^{13}C_{n\text{-alkane}}$ record. This feature may suggest
567 a shift in the dominant sedimentary organic matter source away from freshwater algae

568 to ^{13}C-enriched terrestrial woody organic matter, with HI values of <100 mg HC/g
569 TOC at 2711.4–2712.3m and 2703.5–2706.6m in the lower Da'anzhai Member of
570 Core A, which are much lower than HI values of the upper Da'anzhai Member, where
571 the degree of maturity is similar (Fig. 2; see Supplementary Information for further
572 discussion).

573 Overall, relatively enriched $\delta^{13}C_{TOC}$ values in the more proximal Core B may
574 be explained by the greater woody component of terrestrial residual sedimentary
575 organic matter (the isotopically heavier ligno-cellulose component of a plant)[3,54], as
576 suggested indirectly by low HI values (<200 mg HC/g TOC; Fig. 2) and directly by
577 palynological study (with 26–45% wood). In addition, the more proximal Core B is
578 thermally more mature, with Tmax values mainly of 453–470°C (Tmax values of
579 Core A are mainly 444–460°C). Maturation of kerogen can increase its $\delta^{13}C_{TOC}$
580 values by 1–2‰, which may have further contributed to the offset observed between
581 the organic-carbon isotope records of cores A and B[55]. The observed parallel
582 signature in $\delta^{13}C_{TOC}$ and $\delta^{13}C_{n\text{-alkane}}$ in the main phase of the Da'anzhai Member
583 (above 2698 m) therefore likely reflects a true perturbation of the global exogenic
584 carbon cycle. It is similar in shape and magnitude to what is characteristically
585 observed in lower Toarcian marine calcite and compound-specific marine and
586 terrestrial organic matter from Europe and elsewhere spanning the T-OAE[4,8–10] (Fig.
587 3).

588

589 [3] TERRESTRIAL ENVIRONMENT

590 The consistent superabundance in both cores of the thermophylic pollen genus
591 *Classopollis*, which is thought to have derived from gymnosperm conifers dwelling in
592 regions marginal to bodies of water[32], suggests higher temperature conditions in the

593 continental interior or along the shorelines of the palaeo-Sichuan lake system.
594 Elevated atmospheric and marine temperatures during the T-OAE have also been
595 suggested from coeval marine records, also with increased abundance of *Classopollis*
596 and the ^{18}O-depleted signature of macrofossil calcite[14,18,32].

597

598 **Data availability**

599 The authors declare that the data supporting the findings of this study are available
600 within the article and its supplementary information files.

601

602 45. Ryder, R. T. *Petroleum Geology of the Sichuan Basin, China: Report on U.S.*
603 *Geological Survey and Chinese Ministry of Geology and Mineral Resources Field*
604 *Investigations and Meetings, October 1991*. (U.S. Geological Survey, 1994).
605 46. Li, Y. & He, D. Evolution of tectonic-depositional environment and prototype basins
606 of the Early Jurassic in Sichuan Basin and adjacent areas (in Chinese with English
607 abstract). *Acta Petrolei Sinica* **35**, 219–232 (2014).
608 47. Wall, D. Microplankton, pollen, and spores from the Lower Jurassic in Britain.
609 *Micropaleontology* **11**, 151–190 (1965).
610 48. Dybkjær, K. Palynological zonation and palynofacies investigation of the Fjerritslev
611 Formation (Lower Jurassic-basal Middle Jurassic) in the Danish Subbasin. *Danmarks*
612 *Geologiske Undersøgelse Serie A*, Nr. **30**, 150 p. (1991).
613 49. Bucefalo Palliani, R., Mattioli, E. & Riding, J. B. The response of marine
614 phytoplankton and sedimentary organic matter to the early Toarcian (Lower Jurassic)
615 oceanic anoxic event in northern England. *Mar. Micropaleontol.* **46**, 223–245 (2002).
616 50. Riding, J. B. & Helby, R. Early Jurassic (Toarcian) dinoflagellate cysts from the
617 Timor Sea, Australia. *Memoir of the Association of Australasian Palaeontologists* **24**,
618 1–32 (2001).
619 51. Lichtfouse, E., Derenne, S., Mariotti, A. & Largeau, C. Possible Algal origin of long-
620 chain odd *n*-alkanes in immature sediments as revealed by distributions and carbon-
621 isotope ratios. *Org. Geochem.* **22**, 1023–1027 (1994).
622 52. Meyers, P. Preservation of elemental and isotopic source identification of
623 sedimentary organic matter. *Chem. Geol.* **114**, 289–302 (1994).
624 53. Meyers, P. & Ishiwatari, R. in *Org. Geochem.* Vol. 11 *Topics in Geobiology* (eds.
625 Engel, M. H. & Macko, S.A.) Ch. 8, 185–209 (Springer US, 1993).
626 54. van Bergen, P.F. & Poole, I. Stable carbon isotopes of wood: a clue to palaeoclimate?
627 *Palaeogeogr. Palaeoclimatol. Palaeoecol.* **182**, 31–45 (2002).
628 55. Whelan, J. & Thompson-Rizer, C. in *Org Geochem* Vol. 11 *Topics in Geobiology*
629 (eds. Engel, M.H. & Macko, S.A.) Ch. 14, 289–353 (Springer US, 1993).

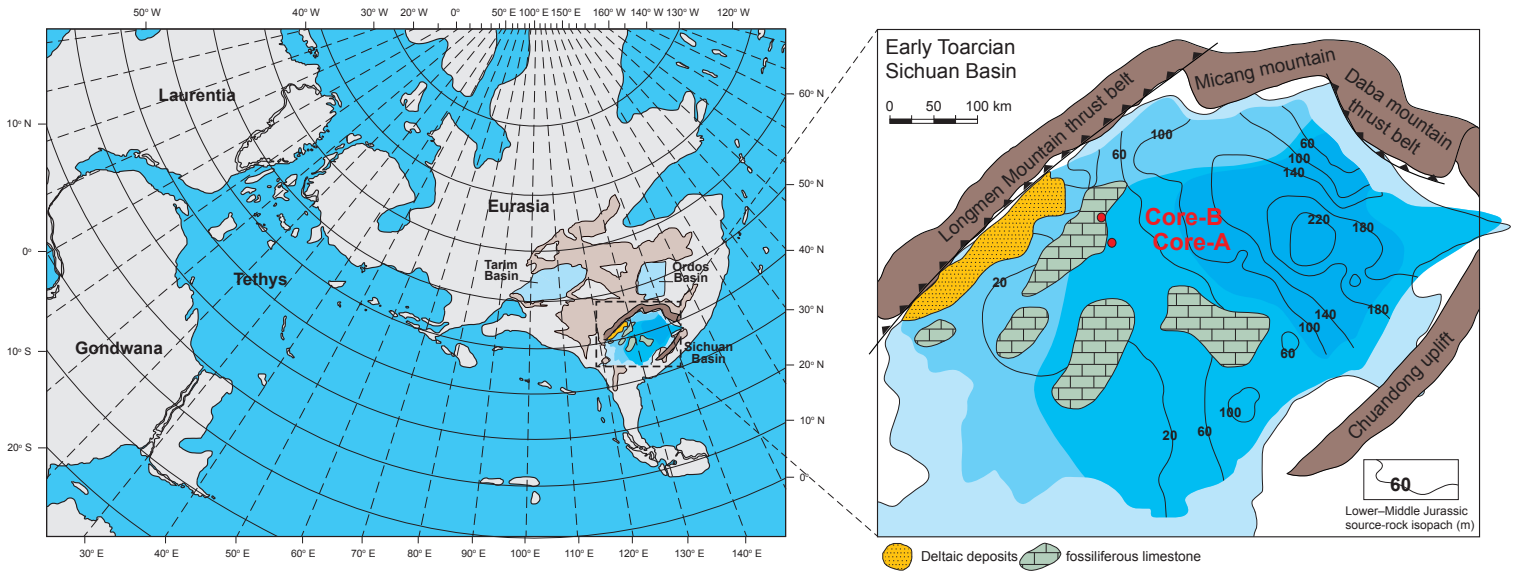
Laurentia
Eurasia
Tethys
Gondwana
Tarim Basin
Ordos Basin
Sichuan Basin
Early Toarcian
Sichuan Basin
0 50 100 km
Longmen Mountain thrust belt
Micang mountain
Daba mountain thrust belt
Chuandong uplift
Core-B
Core-A
60
Lower–Middle Jurassic source-rock isopach (m)
Deltaic deposits
fossiliferous limestone

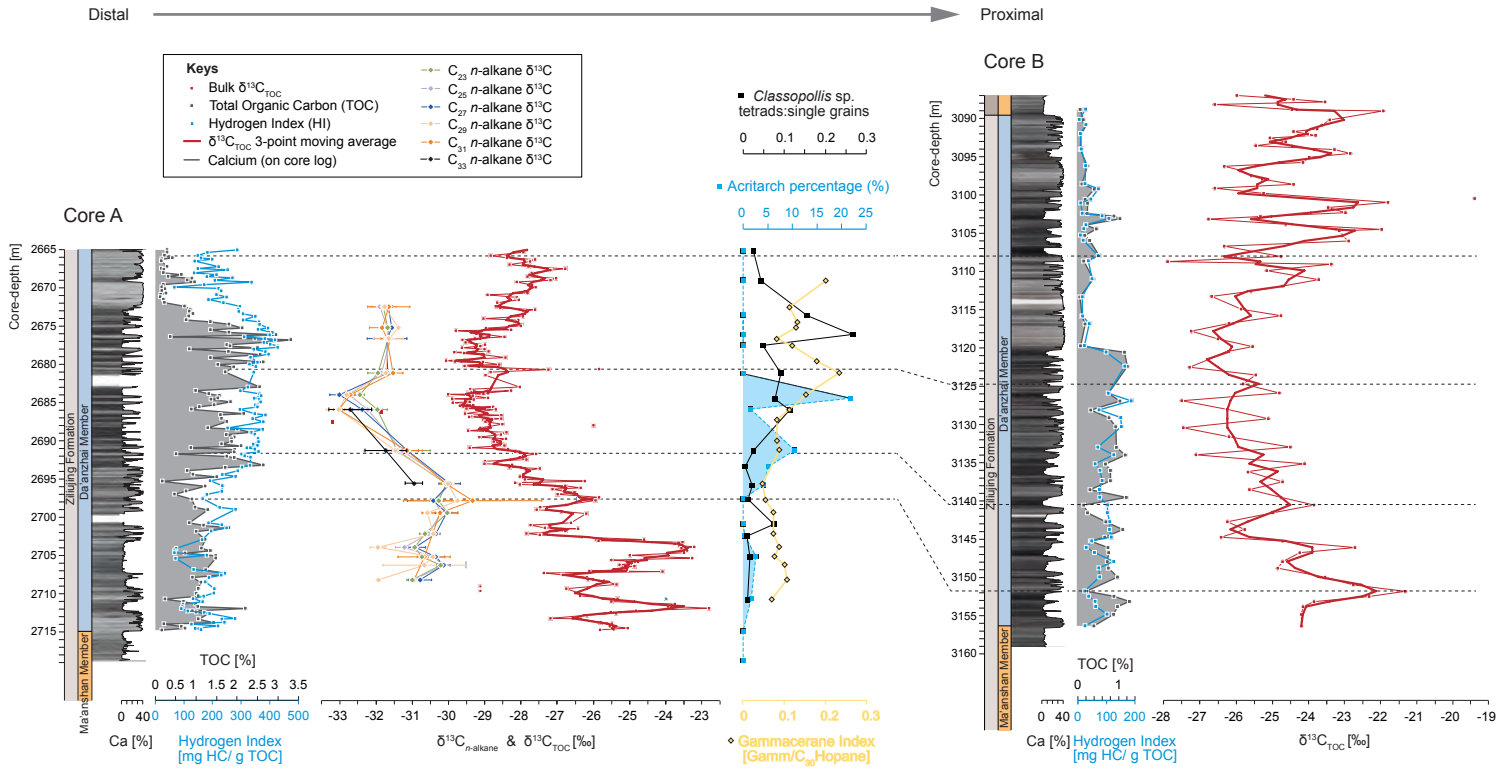
Distal
Proximal
Keys
Bulk δ13CTOC
Total Organic Carbon (TOC)
Hydrogen Index (HI)
δ13CTOC 3-point moving average
Calcium (on core log)
C23 n-alkane δ13C
C25 n-alkane δ13C
C27 n-alkane δ13C
C29 n-alkane δ13C
C31 n-alkane δ13C
C33 n-alkane δ13C
Classopollis sp. tetrads:single grains
Acritarch percentage (%)
Core A
Core B
Core-depth [m]
Zhiluing Formation
Da'anzhai Member
Ma'anshan Member
TOC [%]
Ca [%]
Hydrogen Index [mg HC/ g TOC]
δ13Cn-alkane & δ13CTOC [‰]
Gammacerane Index [Gamm/C30Hopane]
δ13CTOC [‰]

MARINE REALM

Lower Toarcian Marine Black Shales [Yorkshire, UK]

LACUSTRINE REALM

Lower Toarcian Lacustrine Black Shales [Sichuan Basin, China]

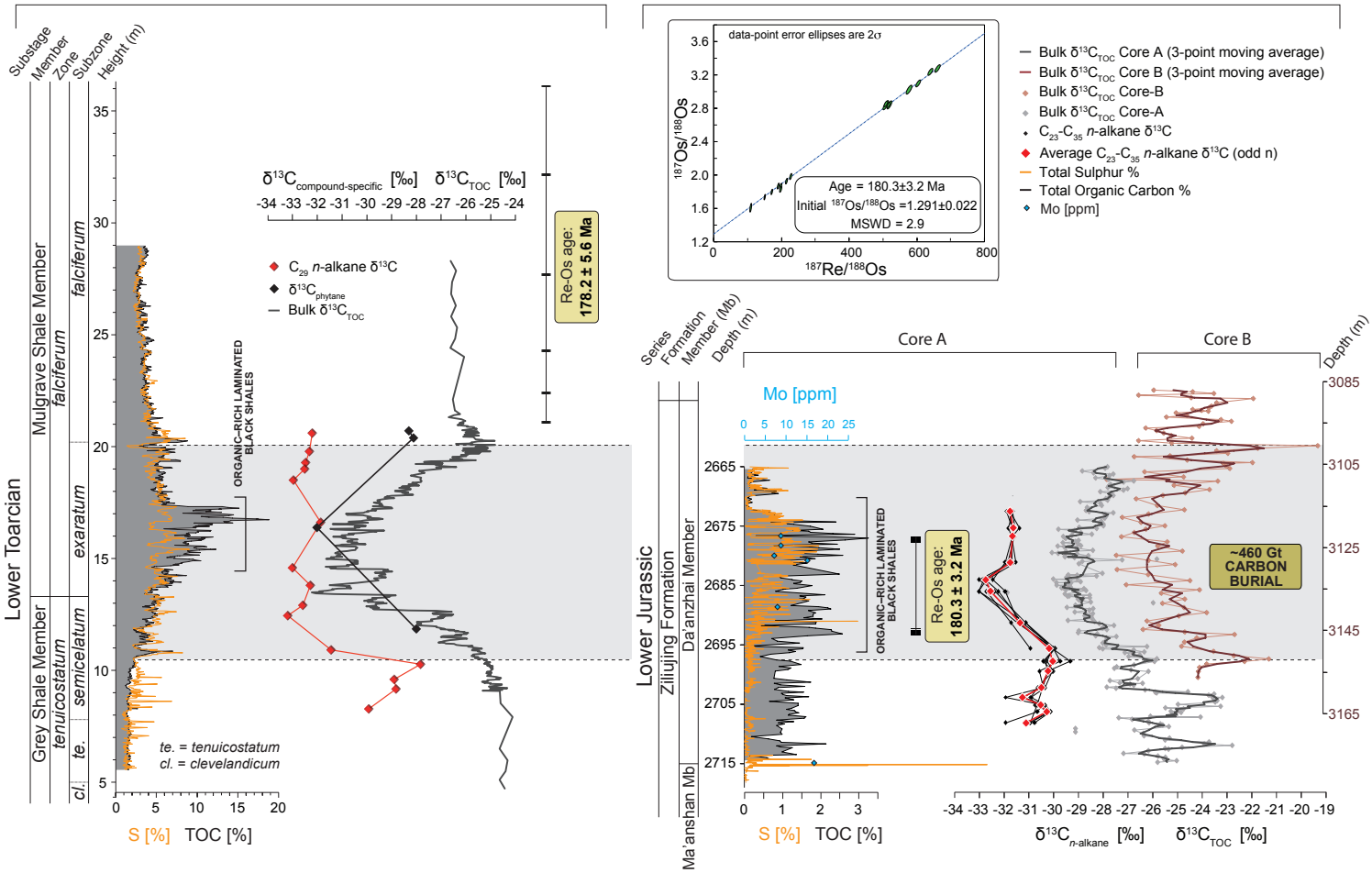

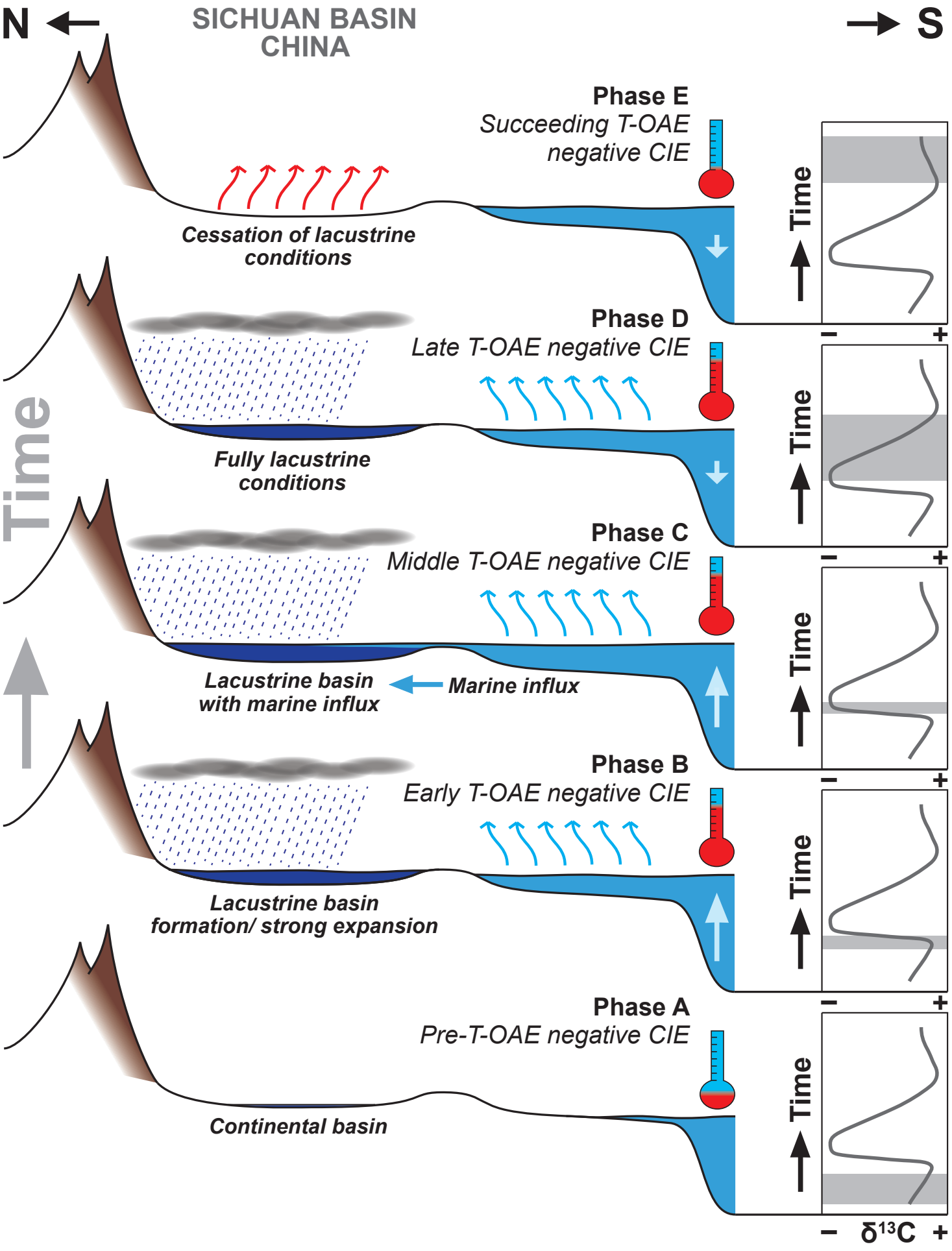
N
SICHUAN BASIN
CHINA
S
Phase E
Succeeding T-OAE
negative CIE
Cessation of lacustrine
conditions
Phase D
Late T-OAE negative CIE
Fully lacustrine
conditions
Phase C
Middle T-OAE negative CIE
Lacustrine basin
with marine influx
Marine influx
Phase B
Early T-OAE negative CIE
Lacustrine basin
formation/ strong expansion
Phase A
Pre-T-OAE negative CIE
Continental basin
Time
Time
Time
Time
Time
Time
Time
– +
– +
– +
– +
– δ13C +

SUPPLEMENTARY INFORMATION

Carbon sequestration in an expanding lake system during the Toarcian Oceanic Anoxic Event

Weimu Xu[1]*, Micha Ruhl[1], Hugh C. Jenkyns[1], Stephen P. Hesselbo[2], James B. Riding[3], David Selby[4], B. David A. Naafs[5], Johan W.H. Weijers[6], Richard D. Pancost[5], Erik W. Tegelaar[6], Erdem F. Idiz[1]

[1]Department of Earth Sciences, University of Oxford, Oxford OX1 3AN, UK (*Correspondence: weimu.xu@earth.ox.ac.uk)

[2]Camborne School of Mines, University of Exeter, Penryn TR10 9FE, UK

[3]British Geological Survey, Keyworth, Nottingham NG12 5GG, UK

[4]Department of Earth Sciences, University of Durham, Durham DH1 3LE, UK

[5]Organic Geochemistry Unit, School of Chemistry and Cabot Institute, University of Bristol, Bristol BS8 1TS, UK

[6]Shell Global Solutions International B.V., Rijswijk 2288 GS, The Netherlands

This file includes:

[1] Methods

[1.1] Materials

Core A is 53.92 m long (from 2665.00 to 2718.92m core-depth), with gaps from 2681.44–2682.84 m and 2699.64–2700.62 m. Core A was sampled at ~25cm resolution. Core B is 72.10 m long (from 3087.00 to 3159.10 m core-depth), with gaps from 3113.64–3114.25 m and 3141.66–3142 m. Core B was sampled at ~80 cm resolution.

[1.2] Rock-Eval pyrolysis

The Rock-Eval 6 Standard Analyzer unit (Vinci Technologies, Nanterre, France), with pyrolysis and oxidation ovens and a flame ionization detector and infra-red cell was used at the Department of Earth Sciences (University of Oxford). S1, S2, Tmax, S3co/S3co$_2$ (New Oxygen Index), S4co/S4co$_2$ (Residual Organic Carbon), S5 (Mineral Carbon) were measured to calculate the Hydrogen Index (HI, in mg HC/g TOC), Mineral Carbon, Oxygen Index, Residual Organic Carbon, TOC. Laboratory procedures from ref. 1 were followed. 45–80 mg of each sample was weighed into crucibles and added to a 48 sample-holder carousel and subsequently run on the machine, with a temperature profile of 300–650 and 300–850°C for the pyrolysis and oxidation ovens, respectively. An IFP 160000 Reference Standard was run once every carousel and the in-house SAB134 (Blue Lias (Jurassic) organic-rich marl) standard was regularly measured every 10 samples on each carousel. The standard deviation on TOC and HI of the in-house SAB134 and the reference IFP160000 standards is 0.065% and 0.066% (TOC) and 22.65 mg HC/g TOC and 10.64 mg HC/g TOC (HI), respectively. The standard deviation on Tmax of the in-house SAB134 is 1.60°C.

[1.3] Hand-Held X-Ray fluorescence (HH-XRF)

Hand-held X-Ray Fluorescence analysis was performed with the Olympus *Innov-X* Delta Premium XRF Analyzer, under climate-controlled laboratory conditions. HH-XRF analyses were executed directly on the flat surface of the slabbed Core A and Core B, at ~5cm resolution throughout the section. The HH-XRF was run in 2 Beam Mining Mode (DS-6000) (each beam a 40-sec measurement window; up to 40 kV) and standard calibration to a manufacturer-delivered standard metal clip was performed at the onset of each run. Additionally, the NIST-2702 and NIST-2781 certified reference standards were regularly measured for quality control on the

measurements, for calibration for long-term drift and measurement offset and to constrain measurement error. Frequent measurements of the NIST-2702 standard show for calcium an average of 0.35% (NIST-2702 = 0.34%), with a standard deviation of 0.01%; for sulphur an average of 0.83% (NIST-2702 = 1.5%), with a standard deviation of 0.01%; and for molybdenum an average of 11ppm (NIST-2702 = 11.4ppm), with a standard deviation of 1.1ppm. Frequent measurements of the NIST-2781 standard show for calcium an average of 4.72% (NIST-2781 = 3.9%), with a standard deviation of 0.05%; for sulphur an average of 1.10%, with a standard deviation of 0.02%, and for molybdenum an average of 26.0ppm (NIST-2781 = 46.7ppm), with a standard deviation of 1.7ppm.

[1.4] Re-Os geochronology

Rhenium-osmium (Re-Os) analysis was conducted for two stratigraphic intervals close to the top and base of the black-shale interval (at 2676.87 to 2677.79 m and 2692.31 to 2693.26 m) in Core A. For each interval, 8 individual horizons, 10 cm apart, were sampled. Samples were crushed at the Department of Earth Sciences, University of Oxford, following the procedures described in ref. 2. The selected core samples were first polished to remove all cutting and drilling marks to eliminate any potential contamination with rhenium or osmium. Samples were subsequently air-dried at 60°C for ~12 hours and broken into rock-chips, without direct metal contact. Samples (1-6 g) were then crushed and homogenized into a fine powder (~30 μm) in a silica mill[3].

Re-Os geochronology was performed at the Laboratory for Sulphide and Source Rock Geochronology and Geochemistry at the Durham Geochemistry Centre, Durham University (UK). The Re and Os from the sample powder was isolated using estimated analytical protocols of refs 2 and 4. In brief, ~0.5g of sample powder, plus a known amount of tracer (spike) solution of ^{190}Os and ^{185}Re was loaded into a carius tube and digested with 8mL of the Cr^{VI}–H_2SO_4 solution for 48 hours at 220°C. The Cr^{VI}–H_2SO_4 solution was used because it could liberate hydrogenous Re and Os preferentially, thereby limiting the incorporation of detrital Re and Os[4–7]. Osmium was extracted from Cr^{VI}–H_2SO_4 solution using the solvent extraction ($CHCl_3$) and further purified using micro-distillation. Rhenium was extracted from the Os-extracted Cr^{VI}–H_2SO_4 solution using NaOH-Acetone extraction, and further purified using anion chromatography.

The purified Re and Os fractions were analyzed for their isotope compositions using negative thermal ionisation mass spectrometry using a ThermoElectron TRITON mass spectrometer via static Faraday collection for Re and ion-counting using a secondary electron multiplier in peak-hopping mode for Os. The Re and Os fractions were loaded onto Ni and Pt filaments, respectively[8]. Total procedural blanks during this study were 12 ± 2 pg and 0.1 ± 0.5 pg (1σ S.D., n = 2) for Re and Os, respectively, with an average $^{187}Os/^{188}Os$ value of 0.25 ± 0.06 (n = 2).

Uncertainties for $^{187}Re/^{188}Os$ and $^{187}Os/^{188}Os$ were determined by full error propagation of uncertainties in Re and Os mass-spectrometer measurements, blank abundances and isotopic compositions, spike calibrations and reproducibility of standard Re and Os isotopic values. The Re-Os isotopic data, including the 2σ calculated uncertainties for $^{187}Re/^{188}Os$ and $^{187}Os/^{188}Os$ and the associated error correlation function (rho), were regressed to yield a Re-Os date using Isoplot V. 4.0 and the λ ^{187}Re constant of $1.666 \times 10^{-11} a^{-1}$ (refs 9–11). The age uncertainty, including the uncertainty of 0.35 % in the ^{187}Re decay constant, only affects the third decimal place[8,11]. Two in-house Re and Os (DROsS) solution standards are analyzed to monitor the long-term reproducibility of mass-spectrometer measurements. For this study, the Re solution standard yields an average $^{185}Re/^{187}Re$ ratio of 0.59841 ± 0.0015 (1 S.D., n = 2), with the Os-isotope reference solution (DROsS) yielding an $^{187}Os/^{188}Os$ ratio of 0.16093 ± 0.00007 (1 S.D., n = 2), which is in agreement with previous studies[12].

[1.5] Palynology

Palynological study was undertaken on 18 samples from Core A and 3 samples from Core B to constrain the age of the sediments and the prevailing palaeoclimatic and palaeoecological conditions. The samples were prepared using the standard acid digestion method including mild oxidation with cold nitric acid[13]; the rock samples, prepared organic residues, and microscope slides are all housed in the collections of the British Geological Survey, Keyworth, Nottingham NG12 5GG, United Kingdom.

[1.6] Bulk organic $\delta^{13}C$ analysis

One gram of homogenized sample was treated with 40mL cold HCl (3 molar) to dissolve the carbonate. Samples (dissolved in 3 molar HCl) were then put on a hot plate for 2 hours at 60°C. Samples were subsequently rinsed 4 times with distilled

water to reach neutral pH. Samples were then oven-dried (at 40°C) and then again powdered. Around 1-15mg (depending on organic-carbon concentration) of homogenized de-carbonated sample residue was weighed into 8×5-mm tin capsules for $\delta^{13}C_{org}$ analyses. The $\delta^{13}C_{org}$ of the samples was measured at the Stable Isotope Laboratory of the Open University (Milton Keynes, UK), with a Thermo Scientific Flash 2000 HT Elemental Analyzer (EA) coupled to a Thermo Scientific MAT253 isotope ratio mass spectrometer via a Conflo IV open split interface. The Thermo Scientific Flash 2000 HT EA has a MAS2000 carousel and between the carousel and the EA sits a Thermo No Blank Device (NBD), allowing for the single sample purging with helium. The EA is also equipped with a Thermal Conductivity Detector (TCD). Automated dilution of sample gas with the Conflo IV open split interface allows for high dynamic range of C+N content and controls the introduction of the "reference" gases. Isotope ratios are reported in standard delta notation relative to Vienna PDB.

Analytical precision was checked with the routine analysis of four internal and referenced laboratory standards (urea 020914MAG, IAEA-CH-6, NIST 8573, IR-R041), showing measured average $\delta^{13}C$ values of -45.24‰, -10.39‰, -26.52‰, -23.58‰, respectively, and standard deviations of 0.85‰, 0.12‰, 0.28‰, 0.49‰.

[1.7] Biomarker analysis

19 samples from Core A were processed for biomarker and compound-specific (C_{23}-C_{33} *n*-alkane) $\delta^{13}C$ analyses. Sample preparation and biomarker analysis were undertaken at the Organic Geochemistry Laboratory facilities at Shell Global Solutions International in Rijswijk (The Netherlands).

[1.7.1] Total lipid extraction

The total lipid fraction of each sample was obtained via extraction using a Dionex ASE® 350 Accelerated Solvent Extractor (ASE). Individual ASE-cells were cleaned with dichloromethane (DCM) and methanol. About 10 grams of powdered and dried sample material was weighed into a cleaned and dried ASE-cell and lipids were subsequently extracted with a 9:1 DCM:methanol solvent mixture in 3 cycles over 45 minutes at a temperature and pressure of 125°C and 1500 psi, respectively. An empty ASE-cell was run at the beginning of each run as a blank and retrieved solvent was checked for molecular contamination. The total lipid extracts (TLEs) were

concentrated to 1 ml in a TurboVap 500 using a helical gas flow and sensor endpoint detection technology. Activated Cu was also added to the extracts to remove any elemental sulphur, which turned out not to be present. Aliquots of the TLE were used for further column chromatography.

[1.7.2] Column chromatography

An aliquot of TLE was separated over $AgNO_3$-impregnated silica gel columns into saturate, aromatic and resin fractions. After pre-conditioning of the column with cyclohexane and application of the TLE, the saturate fraction was eluted with *n*-hexane, the aromatic fraction with toluene and the resin fraction with acetone (3 column volumes each). A mixture of known amounts of standard compounds was added to the aromatic fraction at this stage prior to analysis using Gas Chromatography/Mass Selective Detection. The retrieved saturate fraction of each sample was subsequently separated into *n*-alkane and branched/cyclic alkane fractions.

[1.7.3] *n*-alkane extraction

n-alkanes were extracted from the saturate fraction of each sample using zeolite molecular sieve beads (0.5 nm). The molecular sieve beads were activated in the oven for 3 hours at 120°C, added to the saturate fraction and left standing overnight in cyclo-hexane to trap the *n*-alkane fraction. The cyclohexane, containing the branched/cyclic (b/c) fraction, was transferred to a separate vial and beads were rinsed a few times with cyclohexane, which was added to the b/c fraction. A known amount of standard mixture was added to the b/c fraction at this stage. The b/c fraction was subsequently analyzed using Gas Chromatography/tandem mass spectrometry (GC/MSxMS). A *n*-pentane:cyclo-hexane mixture (88:12) was added to the molecular sieve beads (containing the entrapped *n*-alkanes) and left overnight to release the *n*-alkanes. The *n*-alkane fraction of each sample, dissolved in the *n*-pentane:cyclo-hexane solution, was concentrated and transferred to an autosampler vial. Individual n-alkanes were identified using GC/MS and their carbon-isotope composition was determined using Gas Chromatography/Isotope Ratio Mass Spectrometry (GC/IRMS) (see section [1.8]).

[1.7.4] Biomarker analysis

Aromatic fractions were analyzed for their biomarker content using an Agilent 7890B GC system coupled to an Agilent 5973 mass selective detector (MSD). Separation of compounds was achieved on a J&W DB-1 phase column (60 m × 250 μm, 0.25 μm film thickness) using the following temperature program: 50°C (1 min) - 20°C/min - 120°C - 2°C/min – 320°C (20 min.). The source temperature of the MSD was set at 250°C and it was run in selective ion mode (SIM) scanning for the masses of interest. Compounds were identified in the respective mass chromatograms by comparison of their retention time and elution order with standard samples.

B/c fractions were analyzed for their biomarker content using an Agilent 7890A GC system coupled to an Agilent 7000 Triple Quadrupole Mass Spectrometer. Separation of compounds was achieved on a J&W DB-1 phase column (60 m × 250 μm, 0.25 μm film thickness) using the following temperature program: 50°C (1 min) - 4°C/min - 220°C – 1.2 °C/min – 280°C – 3°C/m – 310°C (20 min.). The temperature of the ion source was set at 250°C and the collision energy in the second quadrupole was set at 10. A selected set of parent–daughter mass transitions was scanned to monitor the compounds of interest. Compounds were identified in the respective mass transition chromatograms by comparison of their retention times and elution order to standard samples. For selected samples the system was run in full scan GC/MS mode to confirm identifications with full mass spectra.

[1.8] Compound-specific (long-chain *n*-alkane) $\delta^{13}C$ analysis

The *n*-alkane fraction was measured for compound-specific $\delta^{13}C$ using an Isoprime 100 GC-combustion-isotope ratio MS (GC-CIRMS) system at the Organic Geochemistry Unit, University of Bristol. Samples were measured in duplicate and $\delta^{13}C$ values were converted to Vienna Peedee Belemnite (VPDB) by bracketing with an in-house gas (CO_2) of known $\delta^{13}C$ value. The reported values are the average of the duplicate measurements. Instrument stability was monitored by regular analysis of an in-house fatty acid methyl ester standard mixture; long-term precision is ± 0.3‰. After injection of 1 or 2 μl onto a Zebron-I non-polar column (50 m length × 0.32 mm diameter × 0.10 μm film thickness), the GC oven program was: 70°C (hold for 1 min) to 130°C at 20°C/min, then to 300°C at 4°C/min, and hold for 25 min. Samples were automatically integrated using the IonVantage software package.

[1.9] Scanning electron microscopy (SEM)

Polished thin-sections (from 2680.4 and 2713.12 m in Core A) were analyzed with a FEI Quanta FEG 650 Scanning Electron Microscope (SEM) at the Department of Earth Sciences, University of Oxford. Back-Scattered Electron Imaging (BSEI) was displayed with brighter regions representing areas with higher average atomic number.

[2] Results

[2.1] Re-Os Geochronology

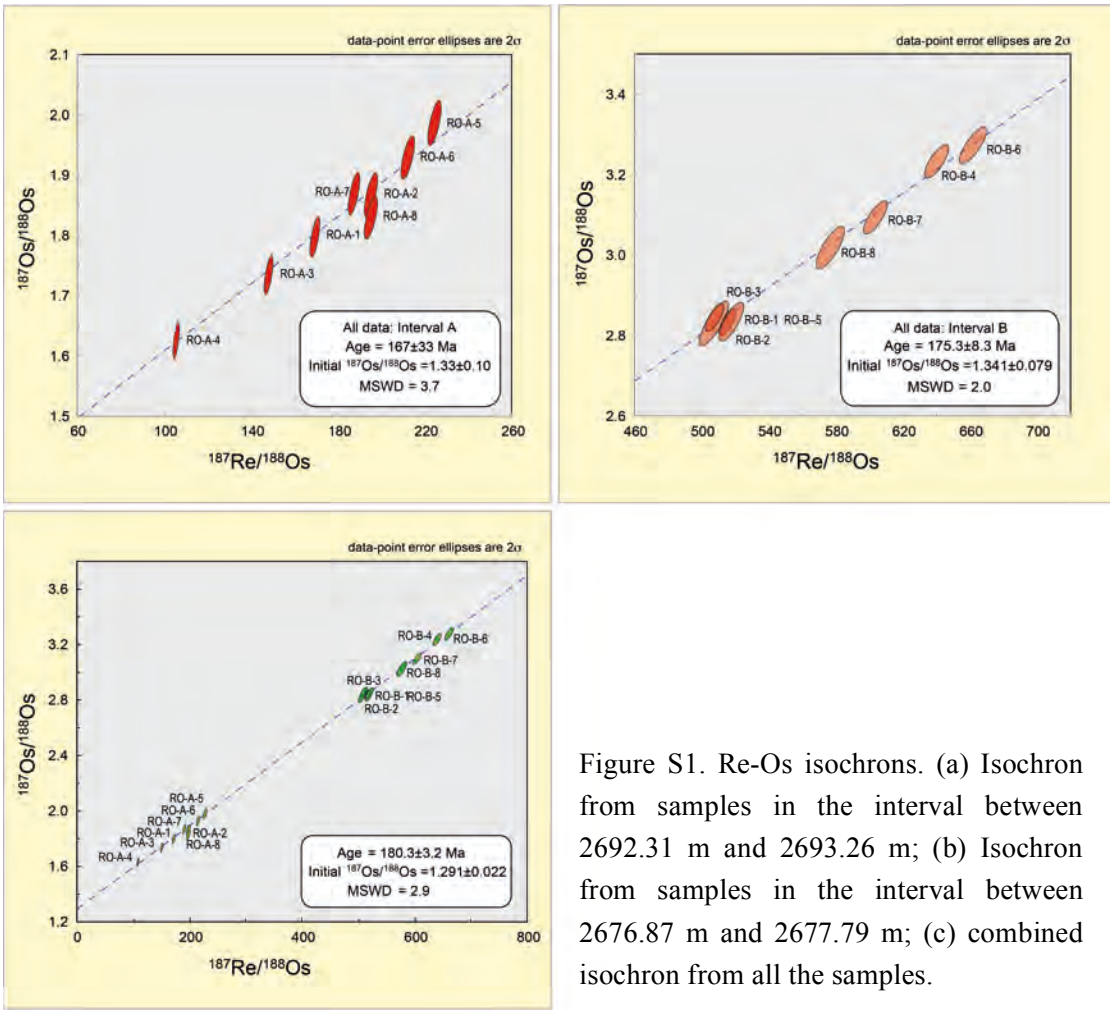

Figure S1. Re-Os isochrons. (a) Isochron from samples in the interval between 2692.31 m and 2693.26 m; (b) Isochron from samples in the interval between 2676.87 m and 2677.79 m; (c) combined isochron from all the samples.

Rhenium-osmium (Re-Os) analysis was conducted for two stratigraphic intervals close to the top and base of the black-shale interval (at 2676.87 to 2677.79 m and 2692.31 to 2693.26 m) in Core A. For each interval, 8 individual horizons, separated by 10 cm, were sampled. The two sampled intervals possess different Re abundances, but similar common Os values (^{192}Os). For example, the interval of 2692.31–2693.26 m possesses 3.5 to 6.8 ppb Re, whereas the interval between 2676.87 m and 2677.79 m contains 9.5 to 22.8 ppb Re, with the ^{192}Os abundances being between 37.3 and

87.9 ppt. Given the difference and similarity in the Re and Os abundances, the Re-Os isotope compositions for the two intervals are distinct.

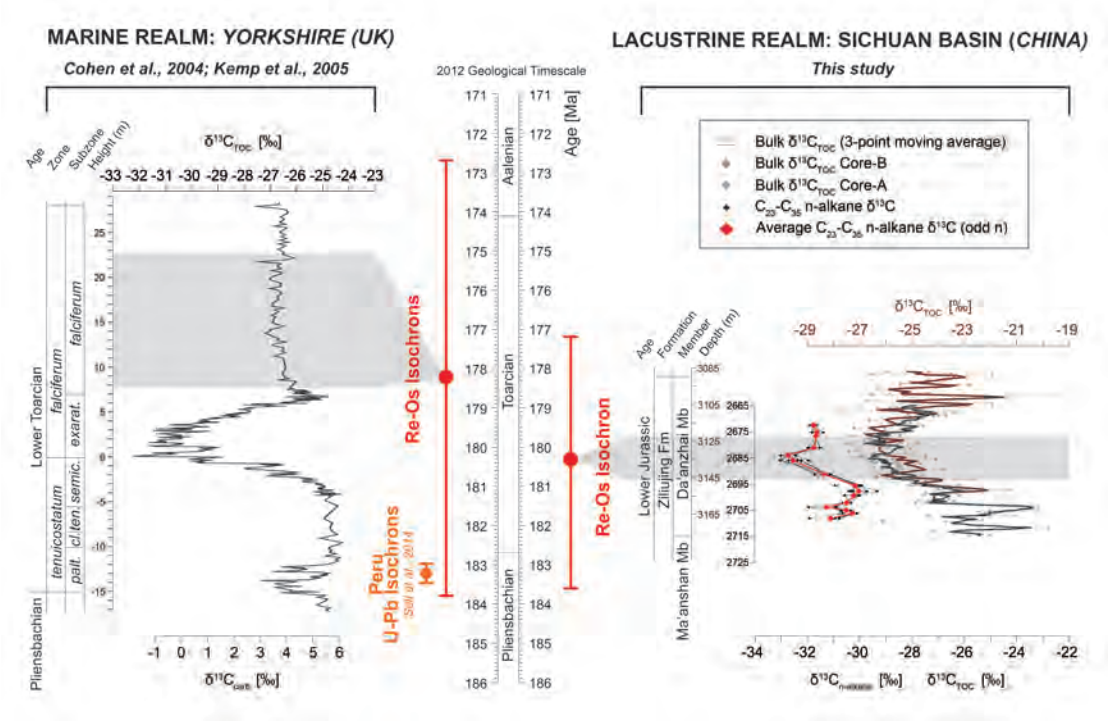

Figure S2. Stratigraphic comparison of the Re-Os ages of the marine Jet Rock in Yorkshire[96] and the lacustrine Da'anzhai Member in this study, relative to the 2012 Geological Time-Scale[97]. The two records are aligned with reference to the negative CIE. The light grey shades represent the stratigraphic intervals from which the samples, used for Re-Os dating, were obtained. Also shown is the U-Pb radiometric age (183.22 ± 0.25 Ma) of an ash-bed in a basal Toarcian marine sedimentary succession (in orange) in the Pucara Basin (Peru), which precedes the T-OAE negative CIE[98]. Although biostratigraphic and chemostratigraphic correlation to the European realm is not straightforward, this basal Toarcian U-Pb radiometric age overlaps, within uncertainty, with the Early Toarcian Re-Os radiometric ages from Yorkshire and the Da'anzhai Member, further constraining the age of the lacustrine Da'anzhai Member.

For samples in the interval between 2692.31 m and 2693.26m, the $^{187}Re/^{188}Os$ values have a relatively small range (~149 and 226 units), and are positively correlated with $^{187}Os/^{188}Os$ values (~1.63 to 1.98). For this sampled interval, 3 samples have very similar Re-Os isotope compositions. All the Re-Os data yield a statistically imprecise Model 3 age of 167 ± 33 Ma (MSWD = 3.7), with an initial $^{187}Os/^{188}Os$ of 1.33 ± 0.10 (Fig. S1 a). Two samples deviate by -0.44 and -2.4 % from the overall regression line (RO-A-2 and RO-A-8). If these two samples are removed from the regression analysis, the Re-Os data yield a Model 1 Re-Os age of 174 ± 14

Ma (MSWD = 1.0), with an initial $^{187}Os/^{188}Os$ of 1.32 ± 0.04. The other sampled interval (2676.87–2677.79 m) also possesses a limited range in the $^{187}Re/^{188}Os$ values (~508 to 662 units). The $^{187}Re/^{188}Os$ data positively correlate with the $^{187}Os/^{188}Os$ data, and yield a Model 3 Re-Os age of 175.3 ± 8.3 Ma (MSWD = 2.0), with an initial $^{187}Os/^{188}Os$ of 1.34 ± 0.08 (Fig. S1 b). Four of the 8 samples yield very similar Re-Os data.

In addition to plotting the data separately, we consider the values as a whole to determine a more statistically meaningful Re-Os date, given: 1) the small amount of geological time between the sampled intervals (both intervals are within the stratigraphic interval of the negative CIE and the duration of the negative CIE has been estimated to be 300–900 kyrs[14-16], which is well below the uncertainty of the Re-Os date; 2) the similar initial $^{187}Os/^{188}Os$ compositions of each sampled interval (Fig. S1 a, b); and 3) the better spread of the range of the Re-Os isotope compositions. Collectively the entire Re-Os data set yields a Model 3 Re-Os age of 180.3 ± 3.2 Ma (MSWD = 2.9), with an initial $^{187}Os/^{188}Os$ of 1.29 ± 0.02 (Fig. S1 c).

A comparison of Early Toarcian Re-Os radiometric ages of the marine Cleveland Basin (Yorkshire, UK) and the lacustrine Sichuan Basin (China) is shown in Figure S2. The obtained Re-Os ages from both settings, albeit from slightly different time-intervals, completely overlap, indicating an Early Toarcian age of the lacustrine Da'anzhai Member in the Sichuan Basin.

[2.2] Palynology

[2.2.1] Core–A

The 18 samples studied for their palynological content produced moderately abundant organic residues that are relatively rich in palynomorphs. The palynofloras are of low diversity; preservation throughout was poor to fair, but this did not prevent identification of the majority of the genera present. The palynomorphs were mid-brown in colour, thereby indicating that the succession examined is moderately thermally mature. The detailed palynological data are outlined in Supplementary Information Table and selected palynomorphs are illustrated in Figure S3.

Gymnosperm pollen, dominantly *Classopollis* spp., comprises between 73.7% and 99.7% of the overall associations; specifically, the 18 samples were overwhelmingly dominated by this Mesozoic pollen genus. An identification to species level was not possible, but the forms are probably largely referable to

Classopollis classoides or *Classopollis meyeriana*. Most specimens were dispersed grains, but some tetrads (groups of four grains) are also present. Other gymnosperm pollen types, present in far lower proportions, comprise undifferentiated bisaccate pollen, *Cerebropollenites macroverrucosus, Chasmatosporites* spp., indeterminate forms, *Perinopollenites elatoides* and *Vitreisporites pallidus*. The specimens of *Chasmatosporites* are commonly somewhat problematical to speciate, but the majority appear to be *Chasmatosporites apertus* or *Chasmatosporites hians.*

Pteridophyte spores are also present in relatively low quantity, and include relatively prominent *Cyathidites* spp. and *Ischyosporites variegatus*. Other spores recorded include *Cibotiumspora juriensis*, *Contignisporites* sp., *Neoraistrickia* sp., *Osmundacidites wellmanii,* indeterminate forms and ?*Kraeuselisporites* sp. Spores are most prominent in the sample at 2714.98 m., comprising 15.0% of the overall assemblage.

Aquatic palynomorphs are relatively sporadic and sparse where present. Acritarchs are only present in Core A and are most prominent (21.9% of the overall palynomorph assemblage) in the sample at 2684.49 m. They, however, mainly occur in the intervals of 2702.49 m to 2710.73 m and 2684.49 m to 2695.8 m and are largely spinose acritarchs, mostly *Micrhystridium* spp., *Veryhachium collectum* and *Veryhachium* spp. Foraminiferal test linings, the dinoflagellate cysts ?*Nannoceratopsis* sp., *Pareodinia halosa* and ?*Skuadinium* sp., and the prasinophyte *Halosphaeropsis liassica* were also encountered.

Amorphous organic material was especially common in the uppermost part of the succession of Core A between 2665.19 m and 2685.94 m. In the lowermost succession, between 2697.7 m and 2718.8 m, woody tissue was the most common kerogen maceral type.

[2.2.2] Core–B

The palynomorphs and the kerogen macerals identified in the 3 samples studied from Core B are depicted in Supplementary Information Table. The palynomorphs are consistently dark brown in colour, indicating that the interval studied is moderately to highly thermally mature. Gymnospermous pollen was again overwhelmingly dominant, comprising between 89.1% and 99.2% of the overall palynofloras. This group is principally represented by *Classopollis* spp., but tetrads of this pollen grain are extremely rare throughout. Bisaccate pollen proved relatively common at 3094.58

m, and *Cerebropollenites macroverrucosus, Chasmatosporites* spp. and *Perinopollenites elatoides* were also found. *Cyathidites* spp. dominate the spore floras, and are most common in the sample at 3094.58m where they make up 10.5% of the terrestrially derived palynomorphs. Other spores are *Contignisporites* sp., *Ischyosporites variegatus, Neoraistrickia* sp. and *Osmundacidites wellmanii*.

Aquatic palynomorphs proved singularly sparse. Such forms are entirely absent in the sample at 3149.9m and single specimens were encountered in the samples at 3094.58m and 3115.65m. A questionable, indeterminate acritarch and one specimen of the freshwater/brackish alga *Botryococcus* are present in the samples at 3115.65m and 3094.58m, respectively. Palynomorphs and woody tissue are generally the most common kerogen macerals. However, amorphous organic material was especially prominent (36% of the overall kerogen) in the sample at 3115.65m.

[2.2.3] Palynostratigraphy

Due to the relatively uniform nature of the palynomorph and kerogen associations within and between the two wells studied, both successions are interpreted as being coeval, and from the same, single genetic sedimentary succession. Despite the relatively low-diversity nature of the palynofloras, and the total dominance of the relatively long-ranging pollen *Classopollis* spp., the assemblages are unequivocally indicative of the Early Jurassic (Early Toarcian). The stratigraphical ranges of selected taxa are illustrated in Figure S4.

The material studied is referable to the Australasian *Classopollis torosa* Oppel Zone, which has been interpreted as being of Hettangian to Early Toarcian age[17] (fig. 46 in ref. 17). The Chinese craton was, during the Jurassic, located across the Tethys Ocean, at a similar palaeolongitude to Australia. *Classopollis classoides* is also typically abundant in the Toarcian of Europe (e.g. refs 18–21)[18–21]. The entire lack of the characteristic Araucarian pollen genus *Callialasporites*, and the absence of significant proportions of typically Middle Jurassic spore genera such as *Leptolepidites* and *Neoraistrickia,* precludes a Middle Jurassic age[22–24] (ref. 22, fig. 3; refs 23 and 24). The range base of the distinctive monosaccate genus *Callialasporites* is close to the Early–Middle Jurassic transition, interpreted as a response to significantly cooler palaeotemperatures in the Middle Jurassic as opposed to the Early Jurassic in Europe. Korte *et al.* (2015) gave a thorough account of the isotopic evidence for this major palaeoclimatic shift[25]. Furthermore, this bio-event appears to

be broadly coeval globally[17,26] (ref. 17, fig. 13; ref. 26). The presence of *Cerebropollenites macroverrucosus* indicates that the succession is no older than Sinemurian age[27,28]. The genus *Chasmatosporites* is also biostratigraphically significant, being a characteristically Lower Jurassic form, and is only infrequently observed stratigraphically higher than the Toarcian[22,29]. Moreover, *Perinopollenites elatoides* is typical of the Early Jurassic in Europe[22,23,30,31].

The pteridopyte spores are also significant in that the association of *Cibotiumspora juriensis*, *Contignisporites* sp. and *Ischyosporites vaerigatus* is consistent with a late Early Jurassic age[32]. The most stratigraphically significant fern spore is *Ischyosporites vaerigatus.* Consistent records of this distinctive, thick-walled, reticulate species, which has affinities to the family Schizaeaceae, range from the Early Jurassic (Pliensbachian–Toarcian transition) to the Early Cretaceous (Albian) of Europe and surrounding regions[33–37]. This species is most prominent in the Middle Jurassic (Aalenian–Bathonian)[18,22,23,30,38,39]. However, the range base of *Ischyosporites vaerigatus* is at the Pliensbachian–Toarcian transition, and the oldest occurrences of consistent records of this species are of earliest Toarcian age. These datum levels were established both in compilations[28,40] (e.g. ref. 28, fig. 4; ref. 40, fig. 5), and by primary studies of well-dated material[33,41–49] (ref. 33, p. 30; ref. 41, table 7; ref. 42, p. 148; ref. 43, figs. 5, 6; ref. 44; ref. 45, p. 815; ref. 46, fig. 6A; ref. 47; ref. 48, fig. 2; ref. 49). Andsbjerg and Dybkjaer (2003, p. 273) stated that the range base of the genus *Ischyosporites* is Toarcian in age[50], although subsequently Barrón et al. (2013, fig. 2) reported an occurrence from the uppermost Pliensbachian of Portugal[48]. Despite the latter record, the best example of this datum in a study using independently dated material was given by Koppelhus and Dam (2003), who undertook a detailed study of the palynology, sedimentology and sequence stratigraphy of the Lower and Middle Jurassic strata of Jameson Land, East Greenland[47]. These authors recorded *Ischyosporites vaerigatus* from the Toarcian successions that they studied[47] (ref. 47, figs. 4A, 10, 12). However, a single-specimen occurrence of *Ischyosporites vaerigatus* was reported from one Sinemurian sample (number 341168). Due to the apparently anomalous nature of this occurrence, this record is deemed to be probably either a misidentification, or the result of contamination. *Ischyosporites vaerigatus* was not recorded throughout the Pliensbachian of East Greenland by Koppelhus and Dam (2003)[47]. However, Guy-Ohlson (1990, table 1) reported very sparse and sporadic occurrences of this species

from the mid–late Pliensbachian of Sweden[51]. There are some sporadic reports of spores assigned to *Ischyosporites* sp. from the Late Pliensbachian of Europe (e.g. ref. 52; ref. 53, fig. 2)[52,53], which may have resulted in the Pliensbachian record of *Ischyosporites vaerigatus* in the compilation of Guy-Ohlson (1989, fig. 3)[54]. To summarize, we contend that there are no reports of consistent occurrences of *Ischyosporites vaerigatus* from strata older than Early Toarcian in the Northern Hemisphere[39]. *Ischyosporites vaerigatus* was also present in Gondwana, and had a similar temporal distribution. Filatoff (1975, figs. 5, 8) reported the range of *Ischyosporites vaerigatus* as being Early Toarcian to Callovian in the Perth Basin, Western Australia[55]. Previously, Balme (1957) had demonstrated that this species occurs throughout the Lower Cretaceous in Western Australia[56].

Wall (1965) demonstrated the abundance and diversity of spinose acritarchs in the Lower Jurassic of the UK[57]. These associations are especially rich in species of *Micrhystridium* and *Veryhachium.* The acritarch species *Veryhachium collectum* was found between 2685.94 m and 2710.73 m in Core A. This taxon was reported from the Pliensbachian by Wall (1965, table 2)[57] and Koppelhus and Dam (2003, fig. 4B)[47]; however, these acritarchs generally range stratigraphically higher than the lowest reported occurrences, so that the presence of *Veryhachium collectum* is deemed to be entirely compatible with an Early Toarcian age of the studied succession.

Dinoflagellate cysts proved relatively rare, another trait of the Lower Toarcian worldwide[58–60]. These palynomorphs are confined to Core A. The occurrences of ?*Nannoceratopsis* and *Pareodinia halosa* are also entirely consistent with an Early Toarcian age[61]. For example, the range base of *Nannoceratopsis* is Upper Pliensbachian[62]. The occurrence of a single specimen of ?*Skuadinium* sp. at 2710.73 m is significant. This genus is distinctively biconical in outline, and was initially described from the Lower Toarcian of the North West Shelf of Australia[63]. The assessment of the Early Toarcian of the *Skuadinium* Suite has been based on the ranges of other dinoflagellate cysts and spores, plus evidence from pollen, foraminifera, calcareous nannofossils and eustasy/sequence stratigraphy[63]. Subsequently, *Skuadinium* was confirmed as a reliable marker for the Lower Toarcian of Australia in a comprehensive review (ref. 60, fig. 8)[60].

Multi-specimen clumps of the prasinophyte species *Halosphaeropsis liassica* were encountered in Core A, albeit rarely, in samples at 2710.73 m, 2702.49 m and 2693.35 m and questionably at 2685.94 m. These occurrences are extremely

significant in that this taxon is typical of marine sediments deposited during the Toarcian Oceanic Anoxic Event (T-OAE) in Europe[44,64–66]. *Halosphaeropsis liassica* was an opportunistic species, which thrived in the environmentally stressed conditions that were developed during the T-OAE[66]. This species has not been reported in significant numbers in sediments other than those deposited during the T-OAE, and is interpreted as being linked to this event in the same way that the dinoflagellate cyst *Apectodinium augustum* is linked to the Paleocene–Eocene Thermal Maximum (PETM)[67,68].

The high levels of amorphous organic material observed between 2665.19 m and 2685.94 m in Core A are consistent with the imprint of the T-OAE in Sichuan Basin strata, with partially degraded biogenic material being abundantly preserved under anoxic conditions[65]. The 18 samples studied here from Core A and 3 samples from Core B are stratigraphically coincident with a marked negative compound-specific and bulk-organic $\delta^{13}C$ excursion, so that the new palynostratigraphy supports the observed negative CIE in the lacustrine Da'anzhai Member to be that of the T-OAE, as recognized in the marine realm.

[2.2.4] Palaeoecology

The occurrences of marine palynomorphs in the samples between 2702.49 m to 2710.73 m and 2684.49 m to 2695.8 m in Core A are unequivocal evidence of marine influence. The marine palynomorphs in these intervals are sufficiently abundant and diverse enough to draw this conclusion. However, where marine forms are sparse, e.g. in the sample at 2702.49 m, the specimens observed may have been introduced by unknown vectors or record reworking or other means of contamination. All the samples that lack marine palynomorphs (i.e. samples at 2718.8 m and 2714.98 m, 2700.9 m and 2697.7 m, and between 2681.17 m and 2665.19 m) are interpreted as representing a definitively lacustrine depositional environment. The occurrence of *Botryococcus*, in the absence of marine palynomorphs, at 3094.58 m in Core B is entirely consistent with a freshwater depositional environment, especially given the palaeontological and organic geochemical evidence.

The dominance of the pollen genus *Classopollis* is clearly significant. Its palaeoecology has been much discussed and it is conventionally interpreted as being thermophilic and a reliable proxy for warm/hot climatic conditions[19,20,69,70]. The parent plants were representatives of the thermophilic and xerophytic family

Cheirolepidiaceae[71]. Vakhrameyev (1970) interpreted the Cheirolepidiaceae as drought-resistant, thermophilous, xerophytic shrubs and trees[72]. The Cheirolepidiaceae have been interpreted to have thrived in coastal and upland slope habitats[55,73]. It appears that the *Classopollis* parent plants lived in a wide variety of habitats that included salt-marsh or mangrove settings under semi-arid to arid conditions.

Chasmatosporites is possibly related to the Order Cycadales[74], representatives of which thrive in modern subtropical and tropical areas. The spore *Ischyosporites variegatus* belongs to the largely tropical Family Schizaeaceae[18]. Hence, much of the non-*Classopollis* pollen and spores are consistent with the evidence for a warm climate provided by the consistent superabundance of *Classopollis* spp.

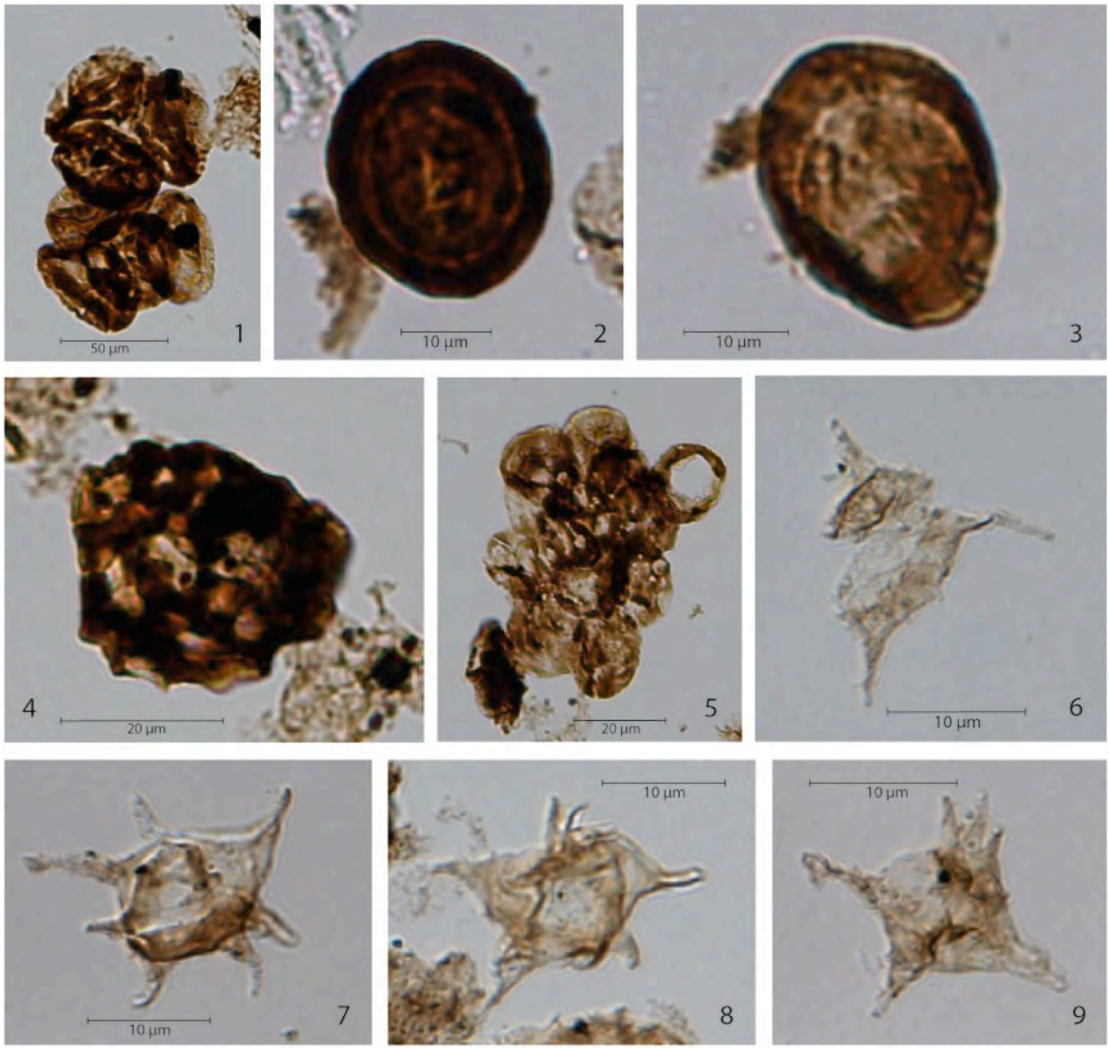

Figure S3. Photomicrographs of selected palynomorphs.

Pollen:

1. Two tetrads of *Classopollis*. 2693.35m Core A. BGS sample MPA 66166/slide 3 at S57/2.
2. *Classopollis* spp. 3094.58m Core B. BGS sample MPA 66168/slide 1 at K39.
3. *Classopollis* spp. 3094.58m Core B. BGS sample MPA 66168/slide 1 at K39.

Spore:

4. *Ischyosporites variegatus* (Couper 1958) Schulz 1967. 2693.35m Core A. BGS sample MPA 66166/slide 3 at S63/4.

Aquatic palynomorphs:

5. A clump of the spherical prasinophyte *Halosphaeropsis liassica* Mädler 1963. 2693.35m Core A. BGS sample MPA 66166/slide 3 at C60/3.
6. *Veryhachium* sp. 2693.35m Core A. BGS sample MPA 66166/slide 3 at E55/4.
7. *Micrhystridium* sp. 2702.49m Core A. BGS sample MPA 66167/slide 1 at O62/3.
8. *Micrhystridium* sp. 2693.35m Core A. BGS sample MPA 66166/slide 4 at M66/4.
9. *Veryhachium collectum* Wall 1965. 2702.49m Core A. BGS sample MPA 66167/slide 1 at R65/1.

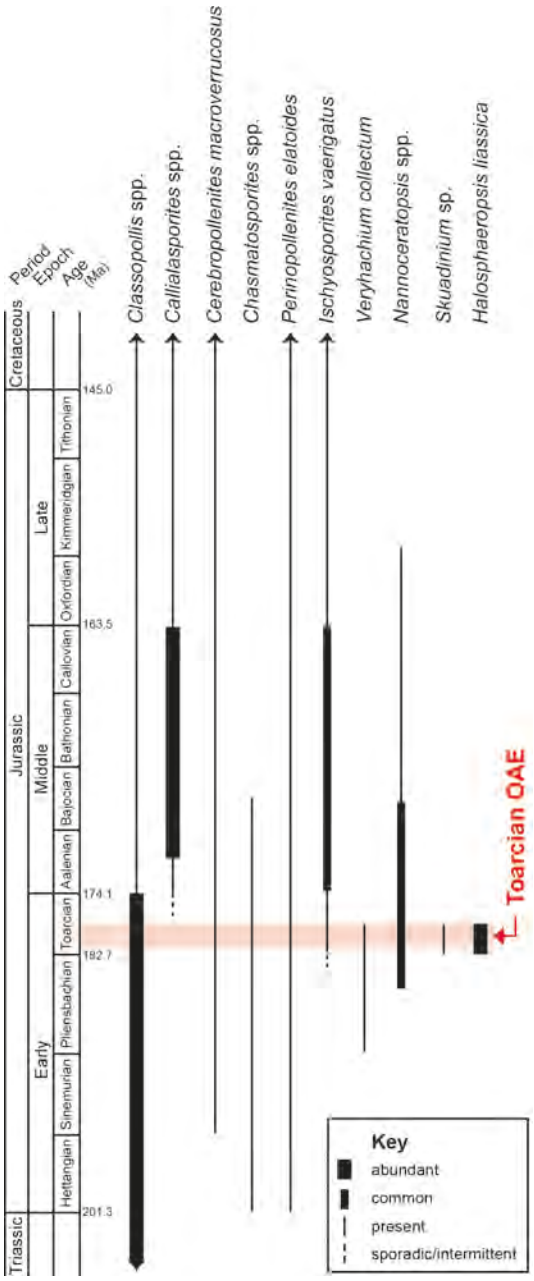

Figure S4. A range chart of selected palynomorphs. This chart illustrates the known semi-quantitative stratigraphical extents of ten selected palynomorph genera and species that were recorded in this study in order to demonstrate the age-diagnostic nature of these forms. These data form part of the basis for the age model in this study and complement Re-Os radiometric age dating and carbon-isotope stratigraphy. The information herein was compiled from works cited in the bibliography.

[2.2.5] Conclusions

The palynology of the 21 samples from Core A and Core B unambiguously defines a stratigraphical interval that corresponds to the Toarcian Oceanic Anoxic Event (T-OAE). The acritarch, dinoflagellate cyst, pollen, prasinophyte and spore floras are all indicative of an Early Toarcian age. Specifically, the occurrences of the acritarch *Veryhachium collectum*, the dinoflagellate cyst ?*Skuadinium* sp., the superabundance of the pollen *Classopollis* spp. (in the absence of *Callialasporites* spp.) and the prasinophyte *Halosphaeropsis liassica*, and the consistent presence of the spore *Ischyosporites vaerigatus* are especially biostratigraphically significant.

Stratigraphic correlation with a negative compound-specific and bulk organic-matter carbon-isotope excursion reinforces this interpretation. The consistent superabundance of the gymnosperm pollen *Classopollis* spp. is indicative of sustained hot/warm climatic conditions. Most samples accumulated in freshwater lacustrine settings, although the presence of acritarchs between 2702.49 m to 2710.73 m and 2684.49 m to 2695.8 m in Core A possibly suggest a transient connection or connections between the lake and the sea.

[2.3] Biomarker analyses

19 samples from Core A were processed for biomarker analyses.

Gammacerane was analyzed by GC/MSxMS parent-daughter mass transition *m/z* 412→191, which also quantifies the 17α-hopane (C_{30} hopane) required for the gammacerane index.

C_{30} tetracyclic polyprenoids (TPP) were detected and analyzed by GC/MSxMS with parent-daughter mass transition *m/z* 414→259 (Fig. S5). The two peaks marked TPPa and TPPb are C_{30} TPP 18α(H), 21R and C30 TPP 18α(H), 21S (ref. 75). The parent-daughter mass transitions *m/z* 372→217, 386→217, 400→217, 414→217 were used to detect C_{27}, C_{28}, C_{29} and C_{30} steranes, respectively.

Two horizons are selected to illustrate the occurrences of TPP and the distribution of steranes. The sample at 2681.17 m contains no marine palynomorphs but displays a high gammacerane index (Fig. 2). The sample at 2691.25 m contains ~10% marine palynomorphs (Fig. 2). TOC of both samples is ~2% and HI values are 301 and 340 mg HC/g TOC, respectively. The sample at 2681.17 m shows a clear presence of TPP (TPP ratio = 0.7), whereas the sample at 2691.25 m shows much lower TPP contents (TPP ratio = 0.3). The sterane distributions are very similar between the two samples. C_{30} steranes (24-*n*-propylcholestanes) are normally sourced from marine algae. The parent-daughter mass transition *m/z* 414→217 does not show any clear peaks in either of the samples analyzed indicating the near absence of C_{30} steranes in both samples despite the fact that one of them contains ~10% marine palynomorphs.

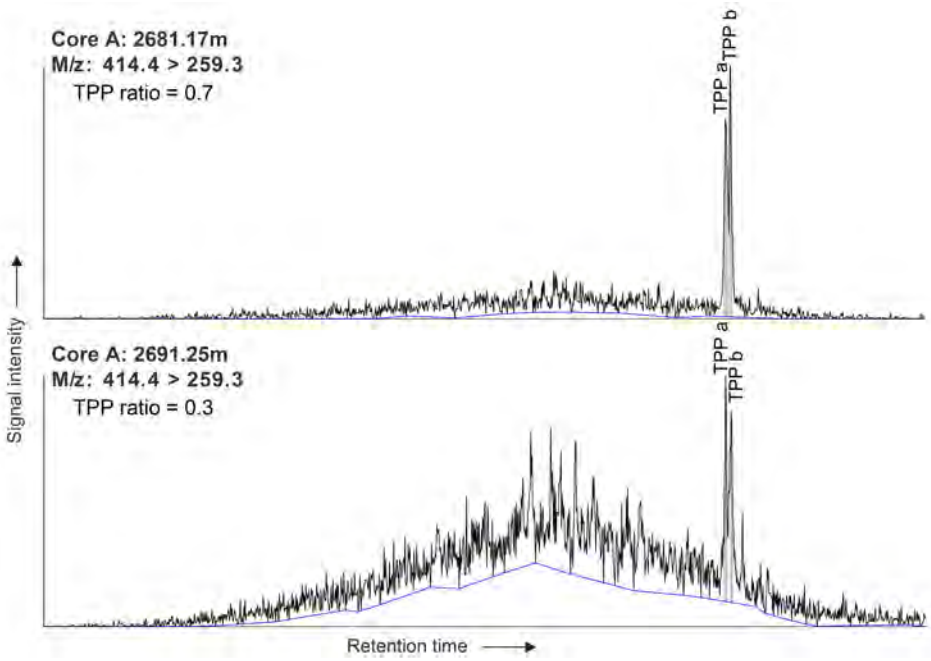

Figure S5. Mass chromatograms of TPP biomarker spectra from core depths 2681.17 m and 2691.25 m in Core A. TPP ratios displayed in the figure are calculated based on Ref. 75.

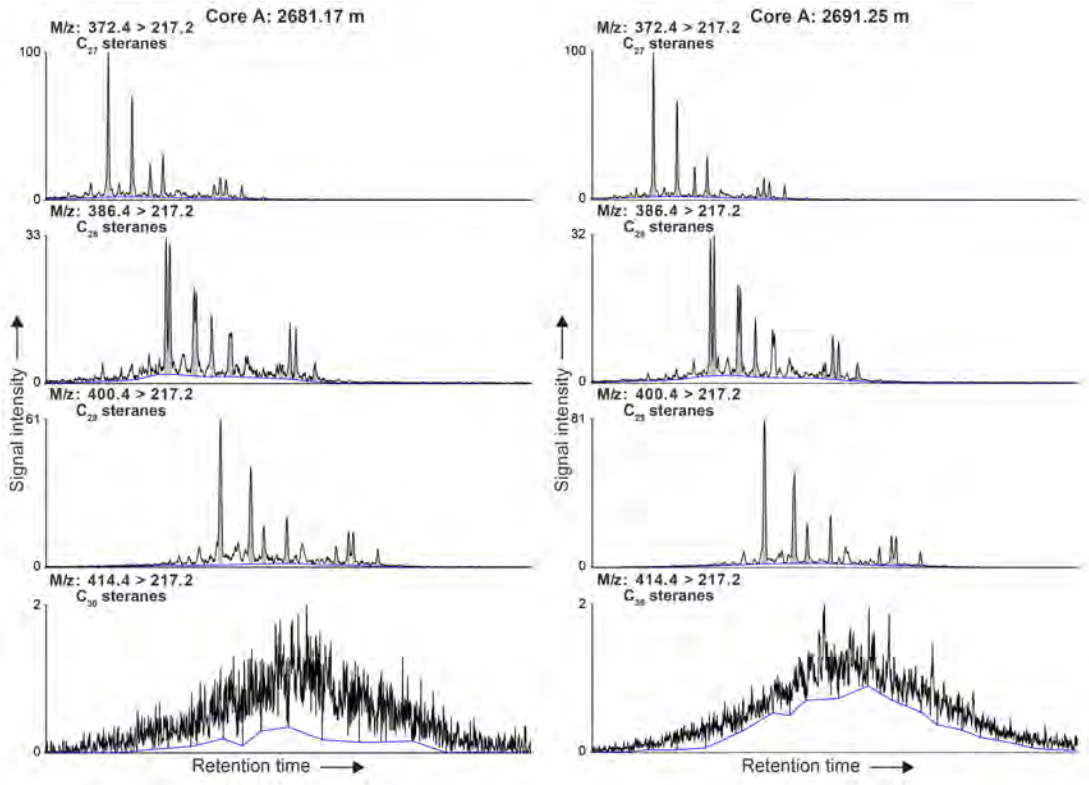

Figure S6. Panels of mass chromatograms of C_{27}, C_{28}, C_{29} and C_{30} steranes from GC/MSxMS data from core depths 2681.17 m and 2691.25 m in Core A. The different transitions from the same sample use the same scale for the *x*-axis.

[2.4] $\delta^{13}C$ *vs* HI &TOC

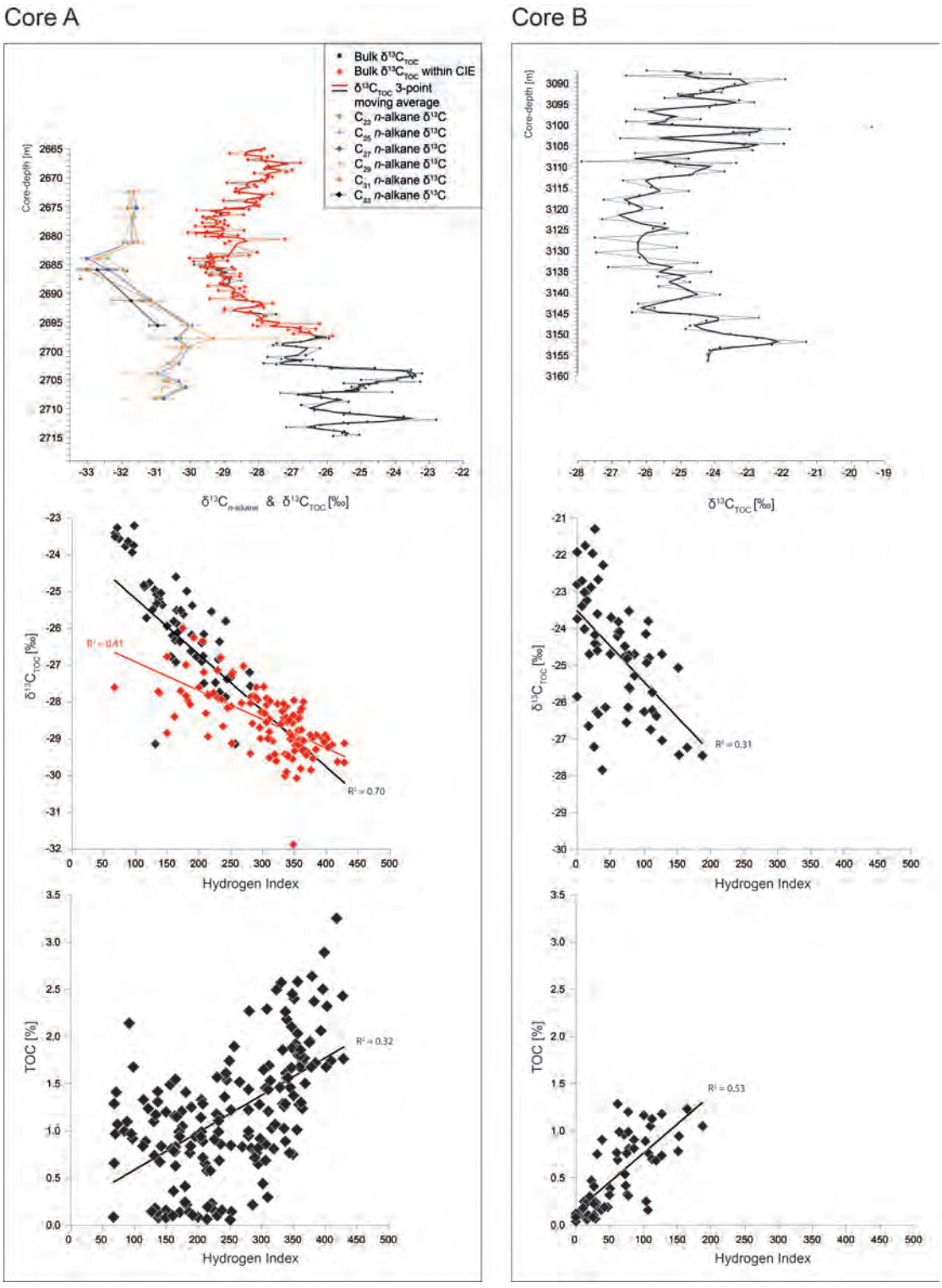

Figure S7. The cross-plot relationships between bulk-organic $\delta^{13}C$ and Hydrogen Index (HI), and bulk-organic $\delta^{13}C$ and Total Organic Carbon (TOC). Specifically, bulk-organic $\delta^{13}C$ within the negative CIE from Core A is marked in red.

Higher plants and marine or freshwater algae fractionate differently for light carbon during photosynthesis, partly depending on environmental background conditions (e.g. atmospheric and aquatic pCO_2). Hydrogen indices (HI) vary depending on the organic-matter precursors as well as subsequent thermogenic or biogenic degradation. A change in the sedimentary organic-matter source may thus be reflected by a change in HI values and (possibly) result in a change in bulk-organic $\delta^{13}C$. A correlation between HI values and $\delta^{13}C_{TOC}$ in a sedimentary record may thus partly reflect organic-matter source mixing, but such interpretation also deserves caution. Tyson (1995) states: "Cross-plots of hydrogen index and $\delta^{13}C$ may show a negligible, weak or strong relationship, depending partly upon whether the variation in HI primarily reflects variable preservation of marine material (and thus redox), or terrestrial-marine mixing due to relative fluxes under moderate to good preservational conditions[76–78]. Where there is no significant variation in $\delta^{13}C$, one can reasonably hypothesize that there was relatively little change in organic matter source, but where $\delta^{13}C$ varies with HI[79–81], it may be unwise to assume that relative terrestrial:phytoplankton ratios are the only factor involved" (ref. 82). He also states: "Isotopic analysis of specific biomarker compounds such as porphyrins, which are believed to preserve their original $\delta^{13}C$ value to within 0.5‰, and comparisons with the bulk TOC $\delta^{13}C$ values, provides a geochemical methodology for appraising diagenetic alteration and mixing effects (refs 83,84)". This methodology has been adopted here, with the bulk $\delta^{13}C_{TOC}$ and the $\delta^{13}C_{n\text{-alkane}}$ records showing a similar ~4‰ negative carbon-isotope-excursion (CIE) during the deepest phase of lake development.

$\delta^{13}C_{TOC}$ and HI values in cores A and B from the Sichuan Basin may correlate overall, but the correlation breaks down when only the interval of the negative carbon-isotope excursion (CIE) is considered, as illustrated in red in Figure S7 (with an R^2 value of only 0.41 for Core A and 0.31 for Core B). Correlation is even poorer between $\delta^{13}C_{TOC}$ and TOC (Figure S7). On the other hand, compound-specific carbon-isotope analysis on long-chain *n*-alkanes, sourced from terrestrial higher-plant leaf waxes or freshwater algae, also shows a 3–4‰ negative excursion, similar in magnitude to that observed in the bulk $\delta^{13}C_{TOC}$ record of the same core and coeval marine successions[85–87]. Aquatic and terrestrial organic matter (e.g. algae, pollen and spores and waxy leaf material) produces relatively high HI values, whereas woody organic matter results in low HI values. Woody organic matter generally also displays

a more positive carbon-isotopic composition. Therefore, sediments showing relatively low HI values (indicating more woody sedimentary organic matter) may also be characterized by more positive carbon-isotope values. Core B shows overall low HI values, suggesting a larger proportion of woody sedimentary organic matter, and possibly explaining the overall more positive signature in bulk $\delta^{13}C_{TOC}$. The ~3‰ fluctuations in bulk $\delta^{13}C_{TOC}$ in the lower part of Core A are not reflected in the $\delta^{13}C_{n\text{-alkane}}$ record and are, therefore, unlikely to reflect global carbon-cycle changes. They may rather reflect source-mixing, as also suggested by the strong correlation between $\delta^{13}C_{TOC}$ and HI values in the interval preceding the CIE, with R^2 = ~0.78.

Correlations between $\delta^{13}C_{TOC}$ and HI values are also widely observed in different marine sections of the T-OAE, where $\delta^{13}C$ of wood or specific compounds already demonstrate the presence of the characteristic carbon-cycle perturbation[86–88]. Comparison of $\delta^{13}C_{TOC}$, $\delta^{13}C_{compound\text{-}specific}$ and HI from Yorkshire, Dotternhausen, Denkingen with the Sichuan Basin (this study; refs 85–89), shows that HI values are strongly elevated up to 800 mg HC/ gTOC in all marine successions (Figure S8 and S9). Irrespective of this high value, compound-specific carbon-isotope records in these marine successions still also show a ~3–4‰ negative excursion, suggesting that changes in the composition of organic matter are not the primary cause of the observed negative CIE (Figure S8). Changes in HI may, however, potentially have slightly altered the magnitude of the negative CIE in bulk $\delta^{13}C_{TOC}$ (ref. 87).

Correction of the bulk $\delta^{13}C_{TOC}$ record for changes in the source of the sedimentary organic matter is, however, not straightforward, especially over major global-change events. Changes in carbon-isotope fractionation in organic matter, under elevated pCO_2, is notoriously poorly constrained, especially in the geological past, and likely differs between major groups of primary producers. As mentioned in the main text, thermal maturity of deeply buried sedimentary rocks can also shift the carbon-isotope composition of bulk $\delta^{13}C_{TOC}$ by 1–2‰ to more positive values[90], with more labile organic matter being more readily influenced by this effect. Furthermore, more labile parts of sedimentary organic matter or compounds are also more easily oxidized depending on the redox state of the depositonal environment. This effect means that the $\delta^{13}C_{TOC}$ and HI values of the preserved organic matter or compounds may have changed non-linearly relative to their original composition. All these factors make it impossible to calibrate reliably, and in detail, the magnitude of global exogenic carbon-cycle change, especially over major events like the T-OAE, based on

simple cross-calibration of bulk $\delta^{13}C_{TOC}$ and HI, and especially when this is based on data pre- or succeeding the event. Therefore, although bulk $\delta^{13}C_{TOC}$ in sediments can be affected by a change in source mixing, the correlative relationship between $\delta^{13}C_{TOC}$ and HI (and its significance, as reflected by R^2 and P-values) cannot be reliably used to compute the magnitude of change in bulk $\delta^{13}C_{TOC}$ due to source mixing. Rather, changes in HI and the carbon-isotope composition of sedimentary organic matter are both consequences of the global climatic perturbation of the T-OAE. Major ^{12}C-enriched carbon release into the ocean-atmosphere system, and associated enhanced hydrological cycling and increased nutrient supply to lacustrine and marine basins, resulted in respectively a major shift in global $\delta^{13}C$ and increased aquatic primary organic productivity with elevated sedimentary HI values.

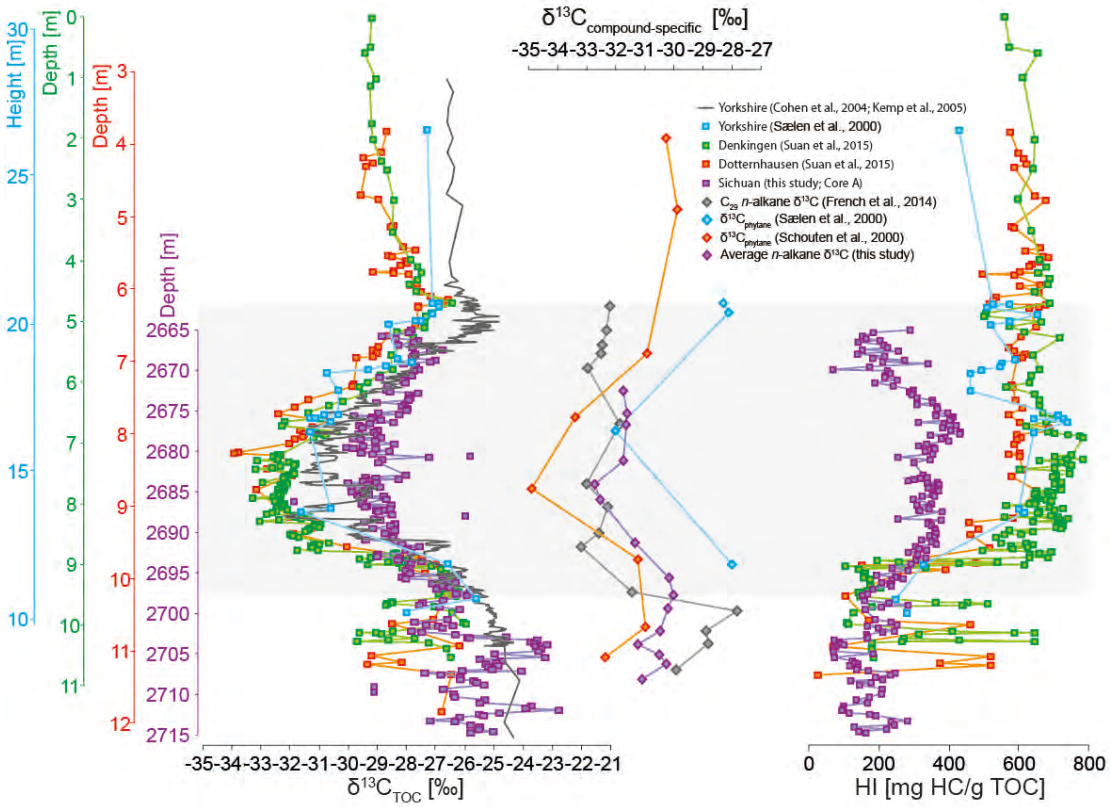

Figure S8. Comparison of the $\delta^{13}C_{TOC}$, $\delta^{13}C_{compound\text{-}specific}$ and HI records from Yorkshire, Dotternhausen, Denkingen and the Sichuan Basin[85–87,89], showing elevated HI values in all marine and lacustrine records, in concert with the T-OAE negative CIEs of ~4–7‰ in $\delta^{13}C_{TOC}$ record and of ~3–4‰ in $\delta^{13}C_{compound\text{-}specific}$ records.

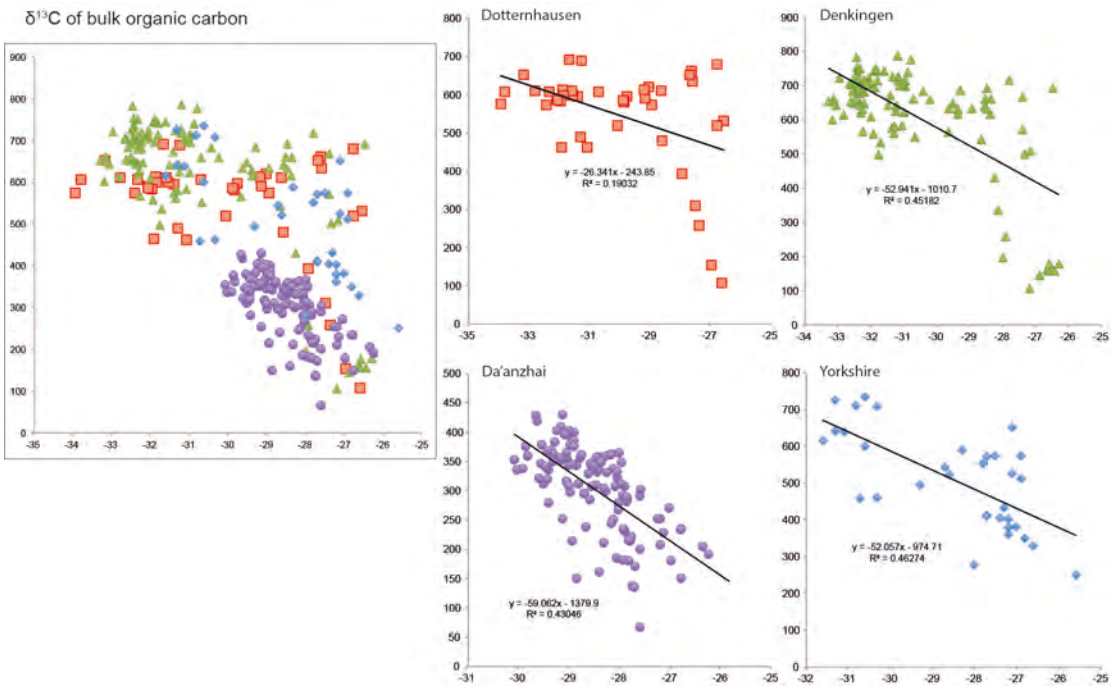

Figure S9. The cross-plot relationships between bulk organic $\delta^{13}C$ and Hydrogen Index (HI) from Yorkshire, Dotternhausen, Denkingen and the Sichuan Basin[85–87,89], showing correlations between bulk-organic $\delta^{13}C$ and Hydrogen Index for all the marine and lacustrine records during the T-OAE negative CIE intervals with, however, a varying magnitude of correlation between different geological settings.

[2.5] Core photo illustration

The core photo in Figure S10 illustrates the transition of sediments from fossiliferous limestone mainly composed of bivalves and ostrocods, to black shale with varying amount of shell fragments, to laminated black shale without any shelly fossils.

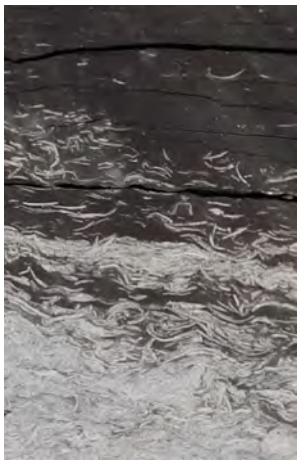

Figure S10. Core photo (oriented) illustrating black shale overlying fossiliferous limestone in Core A.

[2.6] Scanning electron microscopy (SEM)

Two thin-sections (from 2680.4 m and 2713.12 m in Core A), were analyzed with a Scanning Electron Microscope (SEM) FEI Quanta FEG 650. Figure S11 shows examples of observed larger and smaller pyrite (FeS_2) framboids.

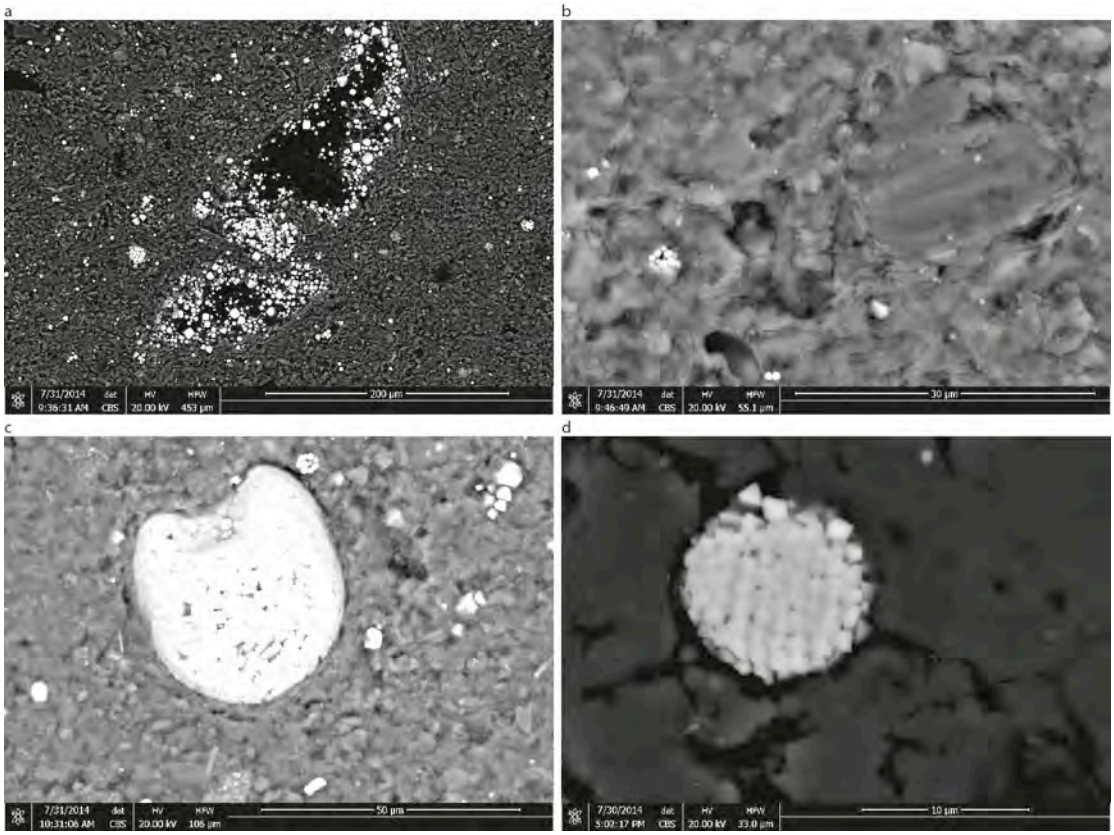

Figure S11. Examples of pyrite framboids from 2680.4 m (a, b, c) and 2713.12 m (d) in Core A, imaged with a back-scattered electron beam detector. (a) Pyrite likely generated by pore-water sulphate reduction due to the oxidation of organic matter. (b) Small (<5 μm) pyrite framboids which may have formed in a euxinic (sulphide-rich) water-column. (c) A fully pyritized shell fragment surrounded by small pyrite framboids. (d) A larger (>5 μm) pyrite framboid, possibly formed during early diagenesis.

[2.7] Mass-balance calculation for the Toarcian global carbon cycle

The amount of total organic-carbon burial in the Da'anzhai Member of the Sichuan Basin alone is estimated using equation (1) and with the following parameters: Area1 (Da'anzhai Member black shales) = 70,000 km^2; Thickness1 = 90 m; TOC1 = 2.2%; Density1 (shale) = 2.6 $\times 10^3$ kg/m^3; Area2 (Da'anzhai Member limestone dominant) = 160,000 km^2; Thickness2 = 50 m; TOC2 = 0.5%; Density2 (limestone) = 2.5 $\times$ 10^3 kg/m^3. With these, the total amount of organic carbon buried in this lake during the T-OAE was estimated to be 460 Gt[91,92] (and this study).

(1) $M_{Sichuan}$ = Area1 * Thickness1 * Density1 * TOC1 + Area2 * Thickness2 * Density2 * TOC2

The amount of total inorganic-carbon burial (M_{IC}) in the Da'anzhai Member of the Sichuan Basin alone is estimated using equation (2), assuming that the Da'anzhai Member over the remaining 160,000 km^2 is on average ~50 m thick and consists on average of about 50% $CaCO_3$ (TC = ~6%). With these, the total amount of inorganic carbon buried in this lake during the T-OAE was estimated to be 1200 Gt.

(2) M_{IC} = Area2 * Thickness2 * Density2 * TC

The total (global) amount of organic (marine + terrestrial) carbon buried is estimated with a simple mass-balance calculation:

(3) $(\delta^{13}C_{Initial} * M_{Initial}) + (\delta^{13}C_{Add} * M_{Add}) - (\delta^{13}C_{TOC} * M_{TOC}) = (\delta^{13}C_{Initial} * (M_{Initial} + M_{Add} - M_{TOC})$

The initial carbon-isotope ratio of the whole exogenic carbon reservoir is taken as $\delta^{13}C_{Initial}$ = 1‰. M_{Add} and $\delta^{13}C_{Add}$ represent the amount and isotopic composition of the carbon released from either ocean-floor methane clathrates (with M_{Add} = 9,000 Gt and $\delta^{13}C_{Add}$ = -60‰) or as thermogenic methane (with M_{Add} = 25,000 Gt and $\delta^{13}C_{Add}$ = -35‰)[93]. Following this and equation (3), the total amount of organic carbon buried (M_{TOC}, with an assumed $\delta^{13}C_{TOC}$ of the burial flux of -25‰), is estimated to be between ~21000 Gt (methane clathrates release model) and ~35000 Gt (thermogenic methane release model). The total amount of organic-carbon burial in the palaeo-Sichuan lake alone is therefore estimated to be 1.3–2.2% of the total (global) organic-carbon burial flux.

Global organic-carbon burial explains the recovery of the global $\delta^{13}C$ signal to more positive values after the initial early Toarcian negative shift. Recovery of the global $\delta^{13}C$ signal would have been delayed if the early Toarcian lacustrine carbon sink in the palaeo-Sichuan Basin had not formed.

(4) $F_{Total} * T_0 = F_{Total\text{-}Sichuan} * (T_0 *(1+ \Delta))$

F_{Total} is the original organic-carbon burial flux; T_0 is the duration of the T-OAE; $F_{Total\text{-}Sichuan}$ is the organic-carbon burial flux without this palaeo-Sichuan lake; and Δ is the % of additional time required to return to the pre-excursion values.

Using equation (4) and with the assumption of constant climatic/environmental parameters affecting the rate of carbon drawdown, we calculate that the early Toarcian global $\delta^{13}C$ signal would have taken 1.3−2.2% additional time to return to pre-excursion values (Figure S12), if the palaeo-Sichuan lake carbon sink had not formed. With an estimated 300−900 kyr duration for the early Toarcian negative CIE, lacustrine carbon sequestration therefore results in a shortening of the observed negative CIE by ~4−20 kyr. These figures are undoubtedly minima, given that several other latest Early Jurassic lacustrine basins containing organic-rich sediments also developed on both the South and the North China Blocks[94,95].

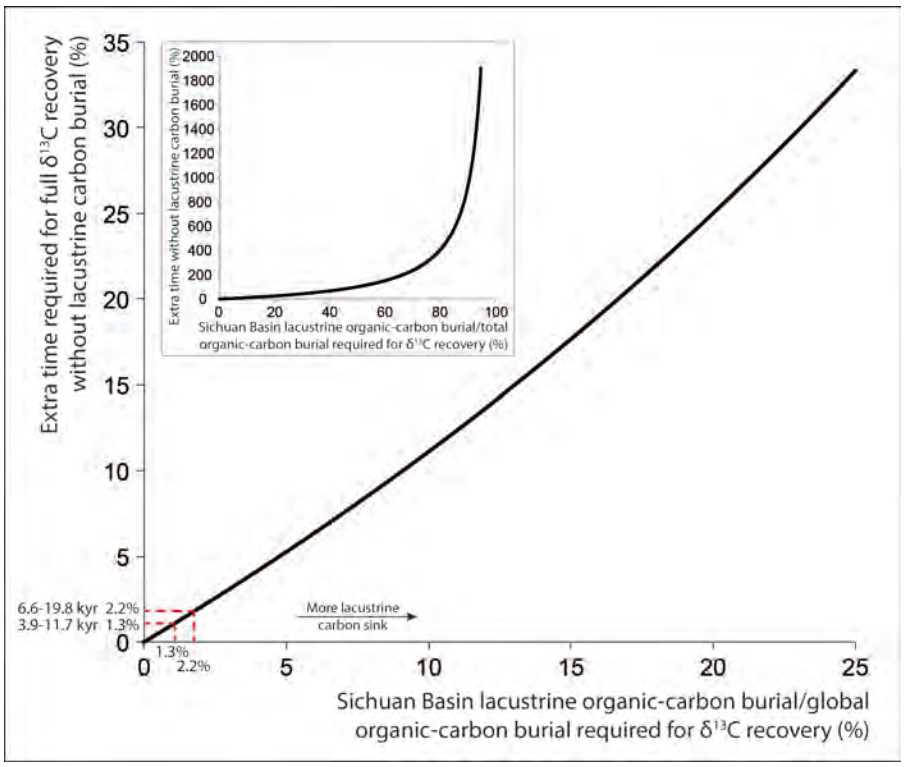

Figure S12. Computed % extra time required for the full recovery of the global $\delta^{13}C$ signal without an Early Toarcian lacustrine carbon sink *vs* the % size of the lacustrine carbon sink relative to global carbon burial. The additional time needed for full recovery of the $\delta^{13}C$ to pre-excursion values, if the lacustrine carbon sinks in the palaeo-Sichuan Basin had not formed, correlates exponentially with the size of the lacustrine carbon sink relative to the global carbon sink.

[3] References

1. Behar, F., Beaumont, V. & De B. Penteado, H.L. Rock-Eval 6 Technology: Performances and Developments. *Oil & Gas Science and Technology – Rev. IFP* **56**, 111–134 (2001).
2. Cumming, V.M., Selby, D. & Lillis, P.G. Re-Os geochronology of the lacustrine Green River Formation: Insights into direct depositional dating of lacustrine successions, Re-Os systematics and paleocontinental weathering. *Earth Planet. Sci. Lett.* **359-360**, 194–205 (2012).
3. Kendall, B., Creaser, R.A. & Selby, D. ^{187}Re-^{187}Os geochronology of Precambrian organic-rich sedimentary rocks. *Geol. Soc. London Spec. Publ.* **326**, 85–107 (2009).
4. Selby, D. & Creaser, R.A. Re-Os geochronology of organic rich sediments: an evaluation of organic matter analysis methods. *Chemical Geology* **200**, 225–240 (2003).
5. Kendall, B.S., Creaser, R.A., Ross, G.M. & Selby, D. Constraints on the timing of Marinoan "Snowball Earth" glaciation by ^{187}Re-^{187}Os dating of a Neoproterozoic, post-glacial black shale in Western Canada. *Earth Planet. Sci. Lett.* **222**, 729–740 (2004).
6. Kendall B., van Acken D. & Creaser R.A. Depositional age of the early Paleoproterozoic Klipputs Member, Nelani Formation (Ghaap Group, Transvaal Supergroup, South Africa) and implications for low-level Re-Os geochronology and Paleoproterozoic global correlations. *Precambrian Research* **237**, 1–12 (2013).
7. Rooney, A.D., Selby, D., Houzay, J.-P. & Renne, P.R. Re-Os geochronology of a Mesoproterozoic sedimentary succession, Taoudeni basin, Mauritania: Implications for basin-wide correlations and Re-Os organic-rich sediments systematics. *Earth Planet. Sci. Lett.* **289**, 486–496 (2010).
8. Selby, D. Direct Rhenium-Osmium age of the Oxfordian-Kimmeridgian boundary, Staffin bay, Isle of Skye, U.K., and the Late Jurassic time scale. *Norw. J. Geol.* **87**, 9 (2007).
9. Ludwig, K.R. Calculation of uncertainties of U-Pb isotope data. *Earth Planet. Sci. Lett.* **46**, 212–220 (1980).
10. Ludwig, K.R. Isoplot version 3.70: a geochronological toolkit for microsoft Excel. *Berkeley Geochronology Center Special Publication No. 4*, 77 (2008).
11. Smoliar, M.I., Walker, R.J. & Morgan, J.W. Re-Os isotope constraints on the age of Group IIA, IIIA, IVA, and IVB iron meteorites. *Science* **271**, 1099–1102 (1996).
12. Du Vivier, A.D.C., Selby, D., Condon, D.J., Takashima, R. & Nishi, H. Pacific ^{187}Os/^{188}Os isotope chemistry and U-Pb geochronology: Synchroneity of global Os isotope change across OAE 2. *Earth Planet. Sci. Lett.* **428**, 204–216 (2015)
13. Wood, G.D., Gabriel, A.M. & Lawson, J.C. in *Palynology: Principles and Applications* v 1 *Palynological techniques—processing and microscopy* (eds Jansonius, J. & McGregor, D.C.) Ch. 3, 29–50 (American Association of Stratigraphic Palynologists Foundation, Dallas, Texas 1996).
14. Kemp, D. B., Coe, A. L., Cohen, A. S. & Weedon, G. P. Astronomical forcing and chronology of the early Toarcian (Early Jurassic) oceanic anoxic event in Yorkshire, UK. *Paleoceanography* **26**, PA4210, doi:10.1029/2011pa002122 (2011).
15. Suan, G. *et al.* Duration of the Early Toarcian carbon isotope excursion deduced from spectral analysis: Consequence for its possible causes. *Earth Planet. Sci. Lett.* **267**, 666–679 (2008).
16. Boulila, S. *et al.* Astronomical calibration of the Toarcian Stage: Implications for sequence stratigraphy and duration of the early Toarcian OAE. *Earth Planet. Sci. Lett.* **386**, 98–111 (2014).
17. Helby, R., Morgan, R. & Partridge, A.D. A palynological zonation of the Australian Mesozoic. *Memoir of the Association of Australasian Palaeontologists* **4**, 1–94 (1987).
18. Couper, R.A. British Mesozoic microspores and pollen grains. *Palaeontographica* Abteilung B **103**, 75–179 (1958).
19. Srivastava, S.K. The fossil pollen genus *Classopollis*. *Lethaia*, **9**, 437–457 (1976).

20. Vakhrameyev, V. A. Pollen *Classopollis*: indicator of Jurassic and Cretaceous climate. *Paleobotanist* **28-29**, 301–307 (1981).
21. Bucefalo Palliani, R. & Riding, J.B. The palynology of the Toarcian–Aalenian transition in the Wittnau borehole (Oberrhein, Southwest Germany). *Neues Jahrbuch für Geologie und Paläontologie Abhandlungen* **210**, 143–184 (1998).
22. Srivastava, S.K. Jurassic spore-pollen assemblages from Normandy (France) and Germany. *Geobios* **20**, 5–79 (1987).
23. Srivastava, S.K. Spore-pollen biostratigraphy of the English Jurassic. *Palaeontographica* Abteilung B **285**, 113–201 (2011).
24. Riding, J.B., Walton, W. & Shaw, D. Toarcian to Bathonian (Jurassic) palynology of the Inner Hebrides, northwest Scotland. *Palynology* **15**, 115–179 (1991).
25. Korte, C. *et al*. Jurassic climate mode governed by ocean gateway. *Nat. Commun.* **6:10015**, doi: 10.1038/ncomms10015 (2015).
26. Quattrocchio, M.E., Volkheimer, W., Borromei, A.M. & Martínez, M.A. Changes of the palynobiotas in the Mesozoic and Cenozoic of Patagonia: a review. *Biol. J. Linnean. Soc.* **103**, 380–396 (2011).
27. Morbey, S.J. & Dunay, R.E. in *Distribution of biostratigraphically diagnostic dinoflagellate cysts and miospores from the northwest European continental shelf and adjacent areas* (ed Thusu, B.) **100**, 47–59 (Continental Shelf Institute Publication, 1978).
28. Dybkjær, K. *Palynological zonation and palynofacies investigation of the Fjerritslev Formation (Lower Jurassic-basal Middle Jurassic) in the Danish Subbasin*. (Danmarks geologiske undersøgelse, 1991).
29. Guy-Ohlson, D. The use of dispersed palynomorphs referable to the formgenus Chasmatosporites (Nilsson) Pocock et Jansonius in Jurassic biostratigraphy. *4o Congreso Argentino de Paleontología y Bioestratigrafía, Mendoza, Actas* **3**, 5–13 (1986a).
30. Weiss, M. Die Sporenfloren aus Rät und Jura Südwest-Deutschlands und ihre Beziehung zur Ammoniten-Stratigraphie. *Palaeontogr. Abt. B* **215**, 1–168 (1989).
31. Riding, J.B., Leng, M.J., Kender, S., Hesselbo, S.P. & Feist-Burkhardt, S. Isotopic and palynological evidence for a new Early Jurassic environmental perturbation. *Palaeogeogr. Palaeoclimatol. Palaeoecol.* **374**, 16–27 (2013).
32. Guy-Ohlson, D. *Jurassic palynology of the Vilhelmsfält Bore No. 1, Scania, Sweden Toarcian-Aalenian*. Section of Palaeobotany Swedish Museum of Natural History, Stockholm, Sweden, 127 (1986b).
33. Schulz, E. & Mai, D.H. Erläuterungen zur Tabelle der stratigraphischen Verbreitung der Sporen und Pollen im Lias und Dogger. *Abhandlungen des Zentrales Geologischen Institüts* **8**, 21–34 (1966).
34. Schulz, E. Sporenpaläontologische Untersuchungen rätoliassischer Schichten im Zentralteil des Germanischen Beckens. *Paläontologische Abhandlungen Abteilung B* **2**, 541–633 (1967).
35. Srivastava, S.K. Microspores from the Fredericksburg Group (Albian) of the southern United States. *Paléobiologie Continentale* **4**, 1–119 (1975).
36. Vigran, J.O. & Thusu, B. Illustrations of Norwegian microfossils. Illustrations and distribution of the Jurassic palynomorphs of Norway. *Royal Norwegian Council for Scientific and Industrial Research (NTNF), Continental Shelf Division Publication* **65**, 55 p (1975).
37. van Erve, A.W. Palynological study of the type localities of the Pliensbachian and Toarcian stages – a preliminary account. *Courier Forschungsinstitut Senckenberg* **34**, 109–116 (1978).
38. Schweitzer, H. J., Ashraf, A.R. & Weiss, M. Korrelation der Sporenzonen der Oberen Trias und des Jura im Mittleren Orient und in Süddeutschland. *Geologische Rundschau* **76**, 923–943 (1987).
39. Mehlqvist, K., Vajda, V. & Larsson, L.M. A Jurassic (Pliensbachian) flora from Bornholm, Denmark – a study of a historic plant-fossil collection at Lund University, Sweden. *GFF* **131**, 137–146 (2009).

40. Shurygin, B.N., Nikitenko, B.L., Il'ina, V.I. & Moskvin, V.I. Problems of stratigraphy of the Lower and Middle Jurassic in the southeastern part of Western Siberia. *Russian Geology and Geophysics* **36**, 35–53 (1995).
41. Herngreen, G.F.W. & de Boer, K.F. Palynology of Rhaetian, Liassic and Dogger strata in the eastern Netherlands. *Geologie en Mijnbouw* **53**, 343–368 (1974).
42. Michelsen, O. Report on the Jurassic of the Hobro No. 1 and Voldum No. 1 borings, Denmark. *Danmarks Geologiske Undersøgelse, Arbog 1978* 141–149 (1979).
43. Hoelstad, T. Palynology of the uppermost Lower to Middle Jurassic strata on Bornholm, Denmark. *Bull. Geol. Soc. Den.* **34**, 111–132 (1985).
44. Lund, J.J. & Pedersen, K.R. Palynology of the marine Jurassic formations in the Vardekløft ravine, Jameson Land, East Greenland. *Bull. Geol. Soc. Den.* **33**, 371–399 (1985).
45. Guy-Ohlson, D. Toarcian palynostratigraphical correlations within and between different biogepgraphical provinces. *2nd International Symposium on Jurassic Stratigraphy, Lisboa* 807–820 (1988).
46. Koppelhus, E.B. & Batten, D.J. Applications of a palynomorph zonation to a series of short borehole sections, Lower to Middle Jurassic, Øresund, Denmark. In *Palynology: Principles and Applications* (eds Jansonius J. & McGregor D.C.) **2,** 779–793 (AASP Foundation, Dallas 1996).
47. Koppelhus, E.B. & Dam, G. Palynostratigraphy and palaeoenvironments of the Rævekøft, Gule Horn and Ostreaelv Formations (Lower-Middle Jurassic), Neill Klinter Group, Jameson Land East Greenland. In *The Jurassic of Denmark and Greenland* (eds Ineson J.R. & Surlyk F.), *Geol. Surv. Den. Greenl.* **1**, 723–775 (2003).
48. Barrón, E., Comas-Rengifo, M.J. & Duarte, L.V. Palynomorph succession of the Upper Pliensbachian–Lower Toarcian of the Peniche section (Portugal). *Communicações Geológicas, 100 Especial* **1**, 55–61 (2013).
49. Mogutcheva, N.K. Main phytostratigraphic boundaries in the Jurassic deposits of Western Siberia. *Stratigr. Geol. Correl.* **22**, 231–238 (2014).
50. Andsbjerg, J. & Dybkjaer, K. Sequence stratigraphy of the Jurassic of the Danish Central Graben. *Geol. Surv. Den. Greenl.* **1**, 265–300 (2003).
51. Guy-Ohlson, D. Pliensbachian palynology of the Karindal bore no. 1, north-west Scania, Sweden. *Rev. Palaeobot. Palynol.* **65**, 217–228 (1990).
52. Rogalska, M. Division of the Liassic deposits in Poland (except for the Carpathian area) based on microscope examinations. *Mémoires du BRGM*, No. 75: 201–210 (1971).
53. Barrón, E., Comas-Rengifo, M.J. & Trincão, P. Estudio palinológico del tránsito Pliensbachiense/ Toarciense en la Rambla del Salto (Sierra Palomera, Teruel, España). *Cuadernos de Geología Ibérica* **25**, 169–185 (1999).
54. Guy-Ohlson, D. In *Northwest European micropalaeontology and palynology* (British Micropalaeontological Society Series) (eds Batten D.J., & Keen M.C.) 70–91 (Ellis Horwood Limited, 1989).
55. Filatoff, J. Jurassic palynology of the Perth Basin, Western Australia. *Palaeontographica* Abteilung B **154**, 1–120 (1975).
56. Balme, B.E. Spores and pollen grains from the Mesozoic of Western Australia. *CSIRO (Commonwealth Scientific and Industrial Research Organisation) Australia Coal Research Section T.C.* **25**, 1–48 (1957).
57. Wall, D. Microplankton, Pollen, and Spores from the Lower Jurassic in Britain. *Micropaleontology* **11**, 151–190 (1965).
58. Woollam, R. & Riding, J.B. Dinoflagellate cyst zonation of the English Jurassic. *Institute of Geological Sciences Report,* 83/2, 42 (1983).
59. Riding, J.B., Fedorova, V.A. & Ilyina, V.I. Jurassic and lowermost Cretaceous dinoflagellate cyst biostratigraphy of the Russian Platform and northern Siberia, Russia. *American Association of Stratigraphic Palynologists Contributions Series* **36**, 179 p (1999).

60. Riding, J.B., Mantle, D.J. & Backhouse, J. A review of the chronostratigraphical ages of Middle Triassic to Late Jurassic dinoflagellate cyst biozones of the North West Shelf of Australia. *Review of Palaeobotany and Palynology* **162**, 543–575 (2010).
61. Prauss, M. Dinozysten-stratigraphie und Palynofazies im Oberen Lias und Dogger von NW-Deutschland. *Palaeontographica* Abteilung B **214**, 1–124 (1989).
62. Riding, J. B. & Thomas, J. E. in *A Stratigraphic Index of Dinoflagellate Cysts* (ed Powell A.J.) 7–97 (Chapman & Hall, 1992).
63. Riding, J. B. & Helby, R. Early Jurassic (Toarcian) dinoflagellate cysts from the Timor Sea, Australia. *Memoir of the Association of Australasian Palaeontologists* **24**, 1–32 (2001).
64. Prauss, M., Ligouis, B. & Luterbacher, H. Organic matter and palynomorphs in the 'Posidonienschiefer' (Toarcian, Lower Jurassic) of southern Germany. In *Modern and Ancient Continental Shelf Anoxia* (eds Tyson R.V. & Pearson T.H.). *Geol. Soc. London Spec. Publ.* **58**, 335–351 (1991).
65. Bucefalo Palliani, R. & Riding, J.B. A palynological investigation of the Lower and lowermost Middle Jurassic strata (Sinemurian to Aalenian) from North Yorkshire, UK. *Proceedings of the Yorkshire Geological Society* **53**, 1–16 (2000).
66. Bucefalo Palliani, R., Mattioli, E. & Riding, J. B. The response of marine phytoplankton and sedimentary organic matter to the early Toarcian (Lower Jurassic) oceanic anoxic event in northern England. *Mar. Micropaleontol.* **46**, 223–245 (2002).
67. Sluijs, A. *et al.* Environmental precursors to light carbon input at the Paleocene/Eocene boundary. *Nature* **450**, 1218–1221 (2007).
68. Kender, S. *et al.* Marine and terrestrial environmental changes in NW Europe preceding carbon release at the Paleocene–Eocene transition. *Earth Planet. Sci. Lett.* **353-354**, 108–120 (2012).
69. Pocock, S.J. & Jansonius, J. The pollen genus *Classopollis* Pflug, 1953. *Micropaleontology* **7**, 439–449 (1961).
70. Volkheimer, W., Rauhut, O.W.M., Quattrocchio, M.E. & Martinez, M.A. Jurassic paleoclimates in Argentina, a review. *Revista de la Asociación Geológica Argentina* **63**, 549–556 (2008).
71. Francis, J.E. The dominant conifer of the Jurassic Purbeck Formation, England. *Palaeontology* **26**, 277–294 (1983).
72. Vakhrameyev, V.A. Range and paleoecology of Mesozoic conifers, the Cheirolepidiaceae. *Paleontolog. J.* **4**, 12–25 (1970).
73. Batten, D.J. Wealden palaeoecology from the distribution of plant fossils. *Proc. Geol. Assoc.* **85**, 433–458 (1975).
74. Pocock, S.J. & Jansonius, J. Redescription of some fossil gymnospermous pollen (*Chasmatosporites, Marsupipollenites, Ovalipollis*). *Canadian Journal of Botany* **47**, 155–165 (1969).
75. Holba, A. G., Tegelaar, E., Ellis, L., Singletary, M. S. & Albrecht, P. Tetracyclic polyprenoids: Indicators of freshwater (lacustrine) algal input. *Geology* **28**, 251–254 (2000).
76. Arthur, M.A., Dean, W.E. & Claypool, G.E. Anomalous ^{13}C enrichment in modern marine organic carbon. *Nature*, **315**, 216–218 (1985).
77. Dean, W.E. & Arthur, M.A. Inorganic and organic geochemistry of Eocene to Cretaceous strata recovered from the lower continental rise, North American Basin, Site 603, Deep Sea Drilling Project Leg 93, in *Initial Reports of the Deep Sea Drilling Project* (eds J.E. van Hinte, S.W. Wise et al.), U.S. Government Printing Office, Washington, DC, **93**, 1093–1137 (1987).
78. Dean, W.E. & Anders, D.E. Effects of source, depositional environment, and diagenesis on characteristics of organic matter in oil shale from the Green River Formation, Wyoming, Utah, and Colorado, in *Geochemical, Biogeochemical, and Sedimentological Studies of the Green River Formation, Wyoming, Utah, and Colorado* (ed. M.L. Tuttle), *United States Geological Survey Bulletin*, **1973-A-G**, F1–F16 (1991).

79. Dean, W.E., Claypool, G.E. & Thiede, J. Accumulation of organic matter in Cretaceous oxygen-deficient depositional environments in the central Pacific Ocean. *Org. Geochem.* **7**, 39–51 (1984).
80. Dean, W.E., Arthur, M.A. & Claypool, G.E. Depletion of ^{13}C in Cretaceous marine organic matter: source, diagenetic, or environmental signal? *Marine Geology* **70**, 119–157 (1986).
81. Moldowan, J.M., Sundararaman, P. & Schoell, M. Sensitivity of biomarker properties to depositional environment and/or source input in the Lower Toarcian of SW-Germany, in Advances in Organic Geochemistry 1985 (eds D. Leythaeuser & J. Rullkötter), Part II, Pergamon, Oxford. *Org. Geochem*. **12**, 915–926 (1986).
82. Tyson, R.V. Bulk geochemical characterization and classification of organic matter: stable carbon isotopes ($\delta^{13}C$), in *Sedimentary organic matter*. pp. 395–416, Chapman & Hall (1995).
83. Hayes, J.M, Popp, B.N., Takigiku, R. & Johanson, M.W. An isotopic study of biogeochemical relationshis between carbonates and organic carbon in the Greenhorn Formation. *Geochim. Cosmochim. Ac.* **53**, 2961–2972 (1989).
84. Takigiku, R., Popp, B.N., Johnson, M.W., Hayes, J.M., Albrecht, P., Callot, H.J. & Ocampo, R. Primary and secondary controls on carbon-isotopic compositions of sedimentary organic matter, in *Diversity of Environmental Biogeochemistry* (ed. J. Berthelin), *Elsevier Developments in Geochemistry*, **6**, 3–14 (1991).
85. Sælen, G., Tyson, R.V., Telnæs, N. & Talbot, M.R. Constracting watermass conditions during deposition of the Whitby Mudstone (Lower Jurassic) and Kimmeridge Clay (Upper Jurassic) formations, UK. *Palaeogeogr. Palaeoclimatol. Palaeoecol.* **163**, 163–196 (2000).
86. French, K.L., Sepúlveda, J., Trabucho-Alexandre, J., Gröcke, D.R. & Summons, R.E. Organic geochemistry of the early Toarcian oceanic anoxic event in Hawsker Bottoms, Yorkshire, England. *Earth Planet. Sci. Lett.* **390**, 116–127 (2014).
87. Suan, G., van de Schootbrugge, B., Adatte, T., Fiebig, J. & Oschmann, W. Calibrating the magnitude of the Toarcian carbon cycle perturbation. *Paleoceanography* **30**, 495–509 (2015).
88. Hesselbo, S. P. *et al.* Massive dissociation of gas hydrate during a Jurassic oceanic anoxic event. *Nature* **406**, 392–395 (2000).
89. Schouten, S., van Kaam-Peters, H.M.E., Rijpstra, W.I.C., Schoell, M. & Sinninghe Damsté, J.S. Effects of an oceanic anoxic event on the stable carbon isotopic composition of Early Toarcian carbon. *American Journal of Science*, **300**, 1–22 (2000).
90. Whelan, J. & Thompson-Rizer, C. in *Org Geochem* Vol. 11 *Topics in Geobiology* (eds. Engel, M.H. & Macko, S.A.) Ch. 14, 289–353 (Springer US, 1993).
91. Zou, C. in *Unconventional Petroleum Geology*. Ch. 3, 61–109 (Petroleum Industry Press, 2013).
92. Li, Y. & He, D. Evolution of tectonic-depositional environment and prototype basins of the Early Jurassic in Sichuan Basin and adjacent areas (in Chinese with English abstract). *Acta Petrolei Sinica* **35**, 219–232 (2014).
93. Beerling, D. J. & Brentnall, S.J. Numerical evaluation of mechanisms driving Early Jurassic changes in global carbon cycling. *Geology* **35**, 247–250 (2007).
94. Huang, K. *et al*. Sedimentary environments and Palaeoclimate of the Triassic and Jurassic in Kuqa River area, Xinjinag (in Chinese with English abstract). *Journal of Palaeogeography* **5**, 197–208 (2003).
95. Yang, Y., Li, W. & Ma, L. Tectonic and stratigraphic controls of hydrocarbon systems in the Ordos basin: A multicycle cratonic basin in central China. *AAPG Bulletin* **89**, 255–269 (2005).
96. Cohen, A. S., Coe, A. L., Harding, S. M. & Schwark, L. Osmium isotope evidence for the regulation of atmospheric CO_2 by continental weathering. *Geology* **32**, 157–160 (2004).
97. Ogg, J. G. & Hinnov, L.A. in *The Geologic Time Scale 2012* Vol. 2 (eds Gradstein, F.M.; Ogg, J.G.; Schmitz, M.D. & Ogg, G.M.) Ch. 26, 731–791 (Elsevier, 2012).

98. Sell, B. *et al.* Evaluating the temporal link between the Karoo LIP and climatic-biologic events of the Toarcian Stage with high-precision U-Pb geochronology. *Earth Planet. Sci. Lett.* **408**, 48–56 (2014).